

Excitation autoionization rates from ground and excited levels in Li-like Ar¹⁵⁺ to S-like Ar²⁺

M. Cohen,* K. B. Fournier, and W. H. Goldstein

Lawrence Livermore National Laboratory, Livermore, California 94550

(Received 14 August 1997)

The rate coefficients for excitation autoionization (EA) from the levels of the ground and first excited configuration in nearly all argon ions (Li-like Ar¹⁵⁺ to S-like Ar²⁺) have been computed. Collisional excitation cross sections are computed in the distorted-wave approximation and integrated over a Maxwellian distribution of free-electron energies. Radiative and autoionizing transition probabilities are computed using the fully relativistic, intermediate coupling code RELAC. For each ion, the rates of EA are compared to semi-empirical calculations of the direct ionization rate. For charge states with few *M*-shell electrons in the ground configuration (Na-, Mg-, and Al-like), EA can significantly enhance the direct ionization rate coefficients. In the first excited configuration of each ion considered, the EA rate coefficient enhances the direct ionization rate coefficient only at low temperatures. [S1050-2947(98)06204-0]

PACS number(s): 34.80.Dp, 34.80.Kw, 32.80.Dz

I. INTRODUCTION

Accurate ionization and recombination rates are necessary for calculations of ion distributions in a plasma. It is well-known from both experimental measurements of total ionization cross sections [1–6] and theoretical investigations [7–22] that indirect processes such as autoionization following electron-impact excitation [excitation autoionization (EA)] make the dominant contribution to some ions' total ionization cross section. In the present work, EA rate coefficients are computed for 14 argon ($Z=18$) ions.

The total cross section for ionization from the ground level in Li-like C³⁺, N⁴⁺, and O⁵⁺ was measured by Crandall *et al.* [1] nearly two decades ago using electron-ion crossed beams. The contribution of EA to the total ionization cross section was identified [1,8] and found to increase in importance along the isosequence [1,2]. The measured data have been used by Sampson and Golden [9,10] to generate analytic formulas for the total ionization cross sections from Li-, Be-, and B-like ions that include terms that account for the EA contribution. The formulas in [10] assume that continuum energy levels have unit autoionization branching ratios; the calculations of the present work reveal that in the case of argon ions, radiative stabilization of inner-shell excited levels substantially reduces the branching ratios in Li-, Be-, and B-like ions.

The Na-like isoelectronic sequence is similar to the Li-like sequence in that there is one electron loosely bound outside a closed shell. Cowan and Mann [7] and LaGattuta and Hahn [11] have calculated that EA is the dominant ionization mechanism in Na-like ions. Recently, the crossed-beam method has been used to measure the Na-like Ar⁷⁺ total ionization cross section up to an impacting-electron energy of 3 keV by Rachafi *et al.* [5] and up to 1200 eV by Zhang *et al.* [6]; the two data sets diverge sharply above impact energies of 375 eV. Many recent calculations [15–17] have interpreted the contribution of EA and resonant

excitation double autoionization (REDA [11]) to the total ionization cross section in Ar⁷⁺; there is reasonable agreement between the total ionization cross sections from the distorted-wave calculations of Reed and Chen [15] and the close-coupling calculations of Tayal [16]; slight differences are due to the number of configurations considered in each model. There are large discrepancies between strengths of the REDA resonances computed in [15] and those computed in [16] that can be traced to differences in the radiative channels allowed for the autoionizing states. The results in Refs. [15] and [16] agree well with the experimental data of Zhang *et al.* [6]. The distorted-wave calculation of the total ionization cross section of Teng and Xu [17] agrees less well with the experiments of Zhang *et al.* [6] than the results in Ref. [15] or [16]. An older work by Sampson [19] offers analytic formulas for the total ionization cross section and the ionization rate coefficient (including contributions from EA) for Na-like ions based on the formalism in Ref. [10], but not informed by the more recent measurements [5,6] above. The EA rates calculated in the present work range from 25% smaller than what is predicted by the formulas in Ref. [19] at 0.6 times the ionization energy of Ar⁷⁺ to only 5% smaller at 2.6 times the ionization energy of Ar⁷⁺. A comparison of the present results with the results of other authors is given in Sec. IV D.

Electron-ion crossed-beam measurements of the total ionization cross section in Ar¹⁺ through Ar⁵⁺ [4] show distinct EA contributions in Ar⁴⁺ (see also [2]) and Ar⁵⁺. The present paper calculates EA rates from levels of the S-, P-, Si-, Al- and Mg-like argon ions. It is similar to our previous work [23] in which the EA contribution to the total rate of ionization was calculated for *M*-shell molybdenum ions. The present work offers systematic calculations of the EA rate coefficient from all levels in the ground configuration of all argon ions from Li-like Ar¹⁵⁺ to S-like Ar²⁺. The present work also offers systematic calculations of the EA rate coefficients from all the levels of the first excited configuration in Li-like Ar¹⁵⁺ to F-like Ar⁹⁺ and Mg-like Ar⁶⁺ to Si-like Ar⁴⁺. Calculations of charge-state distributions [24,25] in low-density plasmas assume that the rate of ionization from the ground level of an ion alone is adequate to describe the

*Permanent address: Racah Institute of Physics, Hebrew University, Jerusalem, Israel.

total rate of ionization from that ion. While this limit obtains in collisionally ionized astrophysical plasmas, for the moderate-density plasmas one finds in magnetically confined fusion devices, this assumption may not apply. For example, the Be-like Ar¹⁴⁺ and Mg-like Ar⁶⁺ ions have metastable levels in their first excited configurations that are close in energy to the ground level and can be highly populated. From collisional-radiative models carried out for the present work, we find that for Be-like Ar¹⁴⁺, at $T_e = 40\%$ of the ion's ionization potential, and for a density typical of a tokamak, 88% of the ion's population is in the ground level and nearly 12% of the ion's population is in the levels of the first excited configuration. For the Mg-like Ar⁶⁺, collisional-radiative models indicate only 55% of the ion's population is in the ground level and nearly 45% of the ion's population is in the levels of the first excited configuration. Comparisons of the calculated EA rate coefficients are made to calculated rate coefficients for impact ionization [26,27] from the valence and inner shells of the same ions (Sec. IV E).

II. EXCITATION AUTOIONIZATION

The cross section for excitation autoionization from a level i of ion $Z+$ to all possible levels of ion $(Z+1)+$ is described by

$$\sigma_i^{\text{EA}} = \sum_j \sigma^{\text{ex}}(i \rightarrow j) B_j^A, \quad (1)$$

where $\sigma^{\text{ex}}(i \rightarrow j)$ is the electron-impact-excitation cross section from level i to level j (an energy level in the continuum of ion Z) and B_j^A is the branching ratio for autoionization from level j to all possible levels of the next ion. In the present work, B_j^A has the form

$$B_j^A = \frac{1}{\Gamma_j^{\text{rad}} + \Gamma_j^A} \left(\Gamma_j^A + \sum_{j'} A_{jj'}^R \frac{\Gamma_{j'}^A}{\Gamma_{j'}^{\text{rad}} + \Gamma_{j'}^A} \right), \quad (2)$$

where Γ_j^{rad} and Γ_j^A represent a sum over all levels reachable from j by radiative transitions and autoionization, respectively,

$$\Gamma_j^{\text{rad}} = \sum_f A_{jf}^R, \quad \Gamma_j^A = \sum_f A_{ji}^A, \quad (3)$$

and $A_{jj'}^R$ is the radiative transition rate from level j to some other level j' , which also lies in the continuum. The second term in the parentheses in Eq. (2) represents the contribution to the total EA rate from autoionization following radiative transitions between energy levels in the continuum. This contribution is found to be negligible for the argon ions studied here. The rate coefficient for the EA process from a specific level i is

$$S_i^{\text{EA}}(T_e) = \sum_j Q_{ij}^{\text{ex}}(T_e) B_j^A, \quad (4)$$

where Q_{ij}^{ex} is the impact-excitation rate coefficient from level i to level j , found by averaging the electron-impact-excitation cross section over a Maxwellian distribution of free-electron velocities

$$Q_{ij}^{\text{ex}}(T_e) = \int_0^\infty v f(v) \sigma^{\text{ex}}(i \rightarrow j) dv, \quad (5)$$

where v is the electron velocity and $f(v)$ is the electron velocity distribution.

III. CALCULATIONS

EA rate coefficients have been calculated for all argon charge states from Ar¹⁵⁺ ($1s^2 2s$, Li-like) to Ar²⁺ ($2s^2 2p^6 3s^2 3p^4$, S-like). The rate of EA from each level in the ground configuration in each ion has been considered as well as the rate of EA from the levels of the first excited configuration, except in the Ne-, Na-, P-, and S-like ions. In the case of Ne-like Ar⁸⁺, the levels of the first excited configuration ($2s^2 2p^5 3s$) are far above the ground level in energy and are not highly populated at the temperatures of interest to the present work. Simple collisional-radiative models for Na-like Ar⁷⁺ have been constructed; the levels of the first excited configuration ($2s^2 2p^6 3p$) have fast radiative decays to the ground level and thus are never highly populated. The code [28] used to calculate the impact-excitation cross sections was unable to converge for excitations from the levels of the first excited configurations in Ar³⁺ and Ar²⁺ and thus no results for the levels of these configurations are reported in the present work.

A. L-shell ions, Ar¹⁵⁺ to Ar⁸⁺

The excitations involved here through which EA proceeds in L-shell argon are listed in Table I. For the Li- and Be-like ions, the promotion of an $n=1$ (K -shell) electron has been allowed according to

$$1s^2 2s^m + e \rightarrow 1s 2s^m n' l' + e, \quad (6)$$

where $m=1$ or 2 for the ground configuration of Ar¹⁵⁺ or Ar¹⁶⁺, respectively, and

$$1s^2 2s^{m-1} 2p + e \rightarrow 1s 2s^{m-1} 2p n' l' + e \quad (7)$$

for the first excited configuration in each ion. For Be-like Ar¹⁴⁺, the contribution to EA from the excitation of a $2s$ electron from the levels of the first excited configuration has also been considered; this is shown in the third line of the Be-like block in Table I. In the case of B-like Ar¹³⁺, the contribution of K -shell excitations to the ground levels EA rates is considered. For all the ions from B-like Ar¹³⁺ to Ne-like Ar⁸⁺, the presence of $2p$ electrons means that excitation of a $2s$ electron can result in autoionizing levels formed from the ground configuration and thus the K -shell excitations contribute only a small fraction to the total EA rate. For these ions, EA from the ground and first excited configurations can proceed via excitations of an $n=2$ (L -shell) electron

$$1s^2 2s^2 2p^k + e \rightarrow (1s^2 2s 2p^k n' l' \text{ or } 1s^2 2s^2 2p^{k-1} n' l') + e, \quad (8)$$

where $k=1-6$ for B- to Ne-like ions, respectively, and from the excited configuration via excitations of the form

TABLE I. *K*- and *L*-shell channels through which EA proceeds for the ground and first excited configurations of Ar¹⁵⁺ to Ar⁸⁺ ions. The first column shows the isoelectronic sequence for the initial ion and the second column contains the electron-impact excitation channels through which EA proceeds. The excitations are listed in order of the excited electron with the innermost excited electron listed first and successive channels having excitations of less bound electrons. The values of *n'l'* considered for each channel are listed to the right of each excitation. The rightmost column of the table lists the final states for autoionization from the excited states in the continuum.

Isosequence	Excitation channel	Final AI states
Li-like	$1s^22s+e \rightarrow 1s2sn'l'$ $1s^22p+e \rightarrow 1s2pn'l'$	$2s \leq n'l' \leq 12g$ $2p \leq n'l' \leq 12g$ $1s^2$ $1s2l, l=0,1^a$
Be-like	$1s^22s^2+e \rightarrow 1s2s^2n'l'$ $1s^22s2p+e \rightarrow 1s2s2pn'l'$ $1s^22s2p+e \rightarrow 1s^22pn'l'$	$2p \leq n'l' \leq 12g$ $2p \leq n'l' \leq 12g$ $10s \leq n'l' \leq 12g$ $1s^2nl, n=2,8; l=0,4$
B-like	$1s^22s^22p+e \rightarrow 1s2s^22pn'l'$ $1s^22s^22p+e \rightarrow 1s^22s2pn'l'$ $1s^22s2p^2+e \rightarrow 1s^22p^2n'l'$	$2p \leq n'l' \leq 8g$ $8s \leq n'l' \leq 11g$ $3p \leq n'l' \leq 11g$ $1s^22snl, n=2,3; l=0,2$
C-like	$2s^22p^2+e \rightarrow 2s2p^2n'l'$ $2s2p^3+e \rightarrow 2p^3n'l'$	$6p \leq n'l' \leq 10g$ $3p \leq n'l' \leq 10g$ $1s^22s^2nl, n=2,3; l=0,2^b$ $1s^22s2p^2$
N-like	$2s^22p^3+e \rightarrow 2s2p^3n'l'$ $2s^22p^3+e \rightarrow 2s^22p^2n'l'$ $2s2p^4+e \rightarrow 2p^4n'l'$	$5s \leq n'l' \leq 10g$ $10s \leq n'l' \leq 10g^c$ $3p \leq n'l' \leq 10g$ $1s^22s^22p^2$ $1s^22s^22p3l, l=0,2^b$ $1s^22s2p^3$
O-like	$2s^22p^4+e \rightarrow 2s2p^4n'l'$ $2s^22p^4+e \rightarrow 2s^22p^3n'l'$ $2s2p^5+e \rightarrow 2p^5n'l'$	$4f \leq n'l' \leq 10g$ $9p \leq n'l' \leq 10g$ $3p \leq n'l' \leq 10g$ $1s^22s^22p^3$ $1s^22s^22p^23l, l=0,2^b$ $1s^22s2p^4$
F-like	$2s^22p^5+e \rightarrow 2s2p^5n'l'$ $2s^22p^5+e \rightarrow 2s^22p^4n'l'$ $2s2p^6+e \rightarrow 2p^6n'l'$	$4d \leq n'l' \leq 11g$ $9s \leq n'l' \leq 11g$ $4s \leq n'l' \leq 11g$ $1s^22s^22p^4$ $1s^22s^22p^33l, l=0,2^b$ $1s^22s2p^5$
Ne-like ^d	$2s^22p^6+e \rightarrow 2s2p^6n'l'$	$4d \leq n'l' \leq 13g$ $1s^22s^22p^5$ $1s^22s2p^6^e$

^aAll $1s2l$ He-like levels are above the highest-energy level of the Li-like ion.

^bAll $n=3$ levels of the Ar^{(Z+1)+} ion are above the highest-energy level of the Ar^{Z+} ion.

^cOnly one level $2s^22p_{1/2}2p_{3/2}10d_{3/2}, J=1/2$ is in the continuum.

^dThe $2s^22p^5n'l'$ levels are below the continuum for all values of $n'l' \leq 13g$.

^eThe $2s2p^6$ F-like level is above the highest-energy level of the Ne-like ion.

$$1s^22s2p^{k+1}+e \rightarrow 1s^22p^{k+1}n'l'+e, \quad (9)$$

where $k=1-5$ for B- to F-like ions, respectively. In Eq. (8), the first configuration on the right-hand side contributes to EA from the levels of the ground and first excited configuration of each ion via a $2s \rightarrow n'l'$ or $2s2p^{k+1} \rightarrow 2s2p^kn'l'$ excitation, respectively. The excitations in Eq. (9) contribute to EA from the levels of the first excited configuration only. The values of $n'l'$ considered for each ion are given in Table I. The continuum levels formed by the above excitations have been allowed to autoionize to all possible states of the next ion. Radiative stabilization of the above levels has been allowed to all possible singly and doubly excited levels of the initial ion.

B. *M*-shell ions, Ar⁷⁺ to Ar²⁺

The allowed excitations for the *M*-shell ions (Ar⁷⁺ to Ar²⁺) considered in the present work are summarized in Table II. For the case of the Na-like Ar⁷⁺, EA proceeds through excitations of the form

$$2s^22p^63s+e \rightarrow 2s^22p^53sn'l' \quad \text{or} \quad 2s2p^63sn'l'+e. \quad (10)$$

For all other *M*-shell ions, Mg-like Ar⁶⁺ to S-like Ar²⁺, excitation of an $n=2$ electron contributes to EA from the ground levels in each ion via inner-shell excited configurations of the form

$$2s^22p^63s^23p^k+e \rightarrow (2l^7)3s^23p^kn'l'+e, \quad (11)$$

TABLE II. *L*- and *M*-shell channels through which EA proceeds for the ground and first excited configurations of Ar⁷⁺ to Ar²⁺ ions. The first column shows the isoelectronic sequence for the initial ion and second column contains the electron-impact excitation channels through which EA proceeds. The excitations are listed in order of the excited electron with the innermost excited electron listed first and successive channels having excitations of less bound electrons. The values of *n'l'* considered for each channel are listed to the right of each excitation. The rightmost column of the table lists the final states for autoionization from the excited states in the continuum.

Isesequence	Excitation channel	Final AI states	
Na-like	$2s^22p^63s + e \rightarrow 2s2p^63sn'l'$ $2s^22p^63s + e \rightarrow 2s^22p^53sn'l'$	$3s \leq n'l' \leq 9g$ $3s \leq n'l' \leq 9g$	$2s^22p^6$ $2s^22p^53l, l=0,2$
Mg-like	$2s^22p^63s^2 + e \rightarrow 2s2p^63s^2n'l'$ $2s^22p^63s^2 + e \rightarrow 2s^22p^53s^2n'l'$ $2s^22p^63s3p + e \rightarrow 2s2p^63s3pn'l'$ $2s^22p^63s3p + e \rightarrow 2s^22p^53s3pn'l'$ $2s^22p^63s3p + e \rightarrow 2s^22p^63pn'l'$	$3p \leq n'l' \leq 8g$ $3p \leq n'l' \leq 8g$ $3p^a \leq n'l' \leq 8g$ $3p^a \leq n'l' \leq 8g$ $6s \leq n'l' \leq 8g$	$2s^22p^6nl, n=3,7; l=0,4$ $2s^22p^53s3l, l=0,2$
Al-like	$2s^22p^63s^23p + e \rightarrow 2s2p^63s^23pn'l'$ $2s^22p^63s^23p + e \rightarrow 2s^22p^53s^23pn'l'$ $2s^22p^63s^23p + e \rightarrow 2s^22p^63s3pn'l'$ $2s^22p^63s3p^2 + e \rightarrow 2s2p^63s3p^2n'l'$ $2s^22p^63s3p^2 + e \rightarrow 2s^22p^53s3p^2n'l'$ $2s^22p^63s3p^2 + e \rightarrow 2s^22p^63p^2n'l'$	$3p \leq n'l' \leq 12i$ $3p \leq n'l' \leq 12i$ $5d \leq n'l' \leq 12i$ $3p^a \leq n'l' \leq 12i$ $3p^a \leq n'l' \leq 12i$ $4s \leq n'l' \leq 12i$	$2p^63snl, n=3,5; l=0,3$
Si-like	$2s^22p^63s^23p^2 + e \rightarrow 2s2p^63s^23p^2n'l'$ $2s^22p^63s^23p^2 + e \rightarrow 2s^22p^53s^23p^2n'l'$ $2s^22p^63s^23p^2 + e \rightarrow 2s^22p^63s3p^2n'l'$ $2s^22p^63s3p^3 + e \rightarrow 2s2p^63s3p^3n'l'$ $2s^22p^63s3p^3 + e \rightarrow 2s^22p^53s3p^3n'l'$ $2s^22p^63s3p^3 + e \rightarrow 2s^22p^63p^3n'l'$	$3p \leq n'l' \leq 12i$ $3p \leq n'l' \leq 12i$ $4d \leq n'l' \leq 12i$ $3p^a \leq n'l' \leq 12i$ $3p^a \leq n'l' \leq 12i$ $4s \leq n'l' \leq 12i$	$3s^2nl, n=3,5; l=0,3$ $3s3p^2$
P-like	$2p^63s^23p^3 + e \rightarrow 2p^53s^23p^3n'l'$ $2p^63s^23p^3 + e \rightarrow 2p^63s3p^3n'l'$ $2p^63s^23p^3 + e \rightarrow 2p^63s^23p^2n'l'$	$3p \leq n'l' \leq 4f$ $3d \leq n'l' \leq 10g$ $6d \leq n'l' \leq 10g$	$3s^23pnl, n=3,4; l=0,3$ $3s3p^3$ $3s3p^23d$
S-like	$2p^63s^23p^4 + e \rightarrow 2p^53s^23p^4n'l'$ $2p^63s^23p^4 + e \rightarrow 2p^63s3p^4n'l'$ $2p^63s^23p^4 + e \rightarrow 2p^63s^23p^3n'l'$	$3p \leq n'l' \leq 4f$ $3d \leq n'l' \leq 8g$ $5p \leq n'l' \leq 10g$	$3s^23p^2nl, n=3,4; l=0,3$ $3s3p^4$ $3s3p^33d$

^a(2l⁷)3s3p^kn'l' with n'l' = 3s is equivalent to (2l⁷)3s²3p^kn'l' with n'l' = 3p (where k=1,2,3 for Mg-, Al-, and Si-like argon). Hence there is no n'l' = 3s considered for the former channel.

where $0 \leq k \leq 4$ for Mg- to S-like argon, respectively. *L*-shell excitations contribute to EA from the levels of the first excited configuration in Mg-, Al-, and Si-like argon ions via

$$2s^22p^63s3p^{k+1} + e \rightarrow (2l^7)3s3p^{k+1}n'l' + e. \quad (12)$$

Promotion of an *M*-shell electron has also been allowed according to

$$(2l)^83s^23p^k + e \rightarrow [(2l)^83s3p^kn'l' \text{ or } (2l)^83s^23p^{k-1}n'l'] + e \quad (13)$$

and

$$(2l)^83s3p^{k+1} + e \rightarrow (2l)^83p^{k+1}n'l' + e. \quad (14)$$

The first configuration on the right-hand side of Eq. (13) can contribute to EA from the levels of the ground configuration through $3s \rightarrow n'l'$ excitations or to EA from the levels of the first excited configuration through $3s3p^{k+1} \rightarrow 3s3p^kn'l'$ excitations, respectively. The excitations in Eq. (14) can only contribute to EA from the levels of the first excited configuration. The values of *n'l'* considered for each ion are given in Table II. The continuum levels formed by the above excitations have been allowed to autoionize to all possible states of the next ion. Radiative stabilization of the above levels has been allowed to all possible singly and doubly excited levels of the initial ion.

C. Atomic structure codes

The atomic structure calculations in the present work are done with the graphical angular momentum coupling code ANGLAR [29] and the fully relativistic parametric potential code RELAC of Klapisch *et al.* [30,31]. RELAC calculates the multiconfiguration, intermediate-coupling energy eigenvalues of the fine-structure levels. Radiative transition rates are then computed for any multipole operator requested [32]. The autoionization rates are found by evaluating the two-electron Coulomb interaction operator between multiconfiguration states of the ion with charge Z and the ion with charge $Z+1$ and a free, outgoing electron [33]

$$A_{jf}^A = \sum_{\tilde{j}} \sum_{J_T, M_T} \left| \left\langle \Psi_f(\Gamma, J) \tilde{j} J_T M_T \left[\sum_{i,j (i < j)} \frac{1}{r_{ij}} \right] \right. \right. \\ \left. \left. \times \left| \Psi_{\beta}(\Gamma'', J'', M_T'') \right. \right. \right|^2, \quad (15)$$

where the state $|\Psi_{\beta}\rangle$ is the multiconfiguration wave function of the initial ion state, $|\Psi_f\rangle$ is the final state in the next ion, and $\tilde{j} = (E_{\tilde{j}}, l_{\tilde{j}}, \tilde{j})$ is a free-electron wave function. The outermost sum in Eq. (15) is over the continuum orbitals making up the partial waves of the outgoing free electron. RELAC uses the factorization technique of Bar-Shalom, Klapisch, and Oreg [28] in Eq. (15) in order to split the matrix element into an angular part depending only on the bound electrons and an interpolation scheme to compute the radial integrals very quickly on a grid of free-electron energies. Details of the procedure and a derivation of the factored form of the transition operator can be found in Ref. [33].

The program CROSS [28] of Bar-Shalom, Klapisch, and Oreg then uses RELAC's wave functions to compute the cross section for impact excitation from energy level i to level j of a given ion in the distorted-wave approximation

$$\sigma^{\text{ex}}(i \rightarrow j) = \frac{2\pi a_0^2}{E_i g_i} \sum_J (2J+1) \\ \times \sum_{\tilde{l}_i, \tilde{l}_j, \tilde{l}_j, \tilde{l}_j} \left| \left\langle \Gamma_j, J_j, \tilde{l}_j, \tilde{l}_j, J \left[\sum_{i,j (i < j)}^{N+1} \frac{1}{r_{ij}} \right] \right. \right. \\ \left. \left. \times \left| \Gamma_i, J_i, \tilde{l}_i, \tilde{l}_i, J \right. \right. \right|^2, \quad (16)$$

where J_i and J_j are the total angular momenta for the initial and final levels, respectively, Γ_i and Γ_j represent all other quantum numbers needed to specify the intermediate-coupling initial and the final levels, respectively, E_i is the incident electron energy in Rydbergs, g_i is the statistical weight of the initial level, \tilde{l}_i and \tilde{l}_j are the orbital angular momenta of the incident and scattered electrons, respectively, and J is the total angular momentum of the target ion plus free-electron system. The two-electron Coulomb interaction operator is evaluated, in this case, between multiconfiguration states of the ion and a free, outgoing electron. The levels of all singly and doubly excited configurations near in energy to the ground configuration have been allowed to mix with each target level. Thus, for example, mixing from $(2l)^8 3p^2$, $(2l)^8 3p3d$, and $(2l)^8 3d^2$ has been included in the calculation of the excitation rate coefficient from the levels of $(2l)^8 3s^2$ and $(2l)^8 3s3p$ in Ar^{6+} and mixing of $1s^2 2p^3$ has been included in the calculation of the excitation rate coefficient from the levels of $1s^2 2s^2 2p$ in Ar^{13+} . Higher-energy bound states, which are needed for radiative stabilization of the autoionizing levels (discussed below), are also allowed to mix with each target level.

IV. RESULTS AND DISCUSSION

A. L-shell ions

The EA rate coefficients from the ground level of the L-shell argon ions are shown in Fig. 1. The EA rate coeffi-

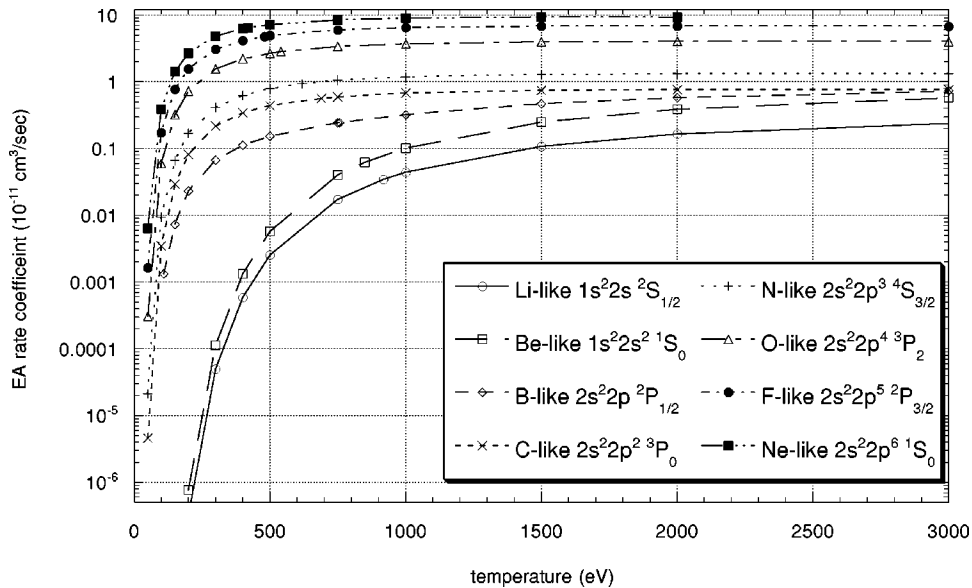


FIG. 1. EA rate coefficients for the ground level in each L-shell argon ion as a function of temperature.

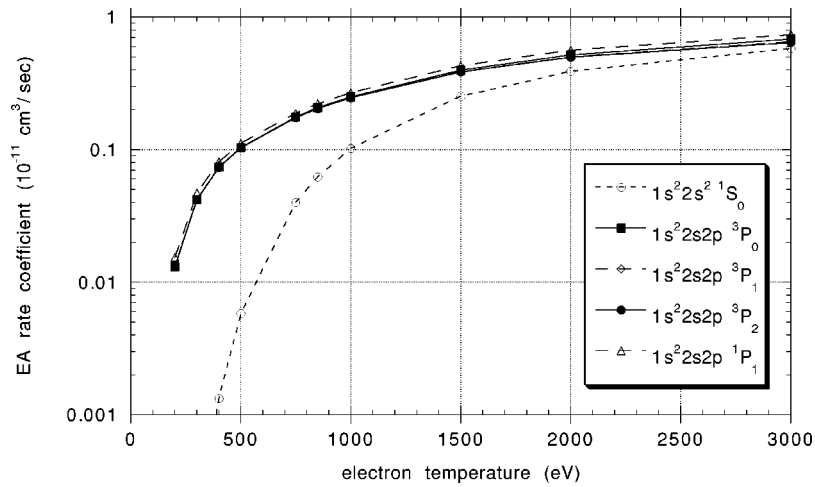


FIG. 2. EA rate coefficient for the Be-like Ar^{14+} $2s^2 \ ^1S_0$ ground and $2s2p$ ($^3P_{0,1,2}$ and 1P_1) excited energy levels.

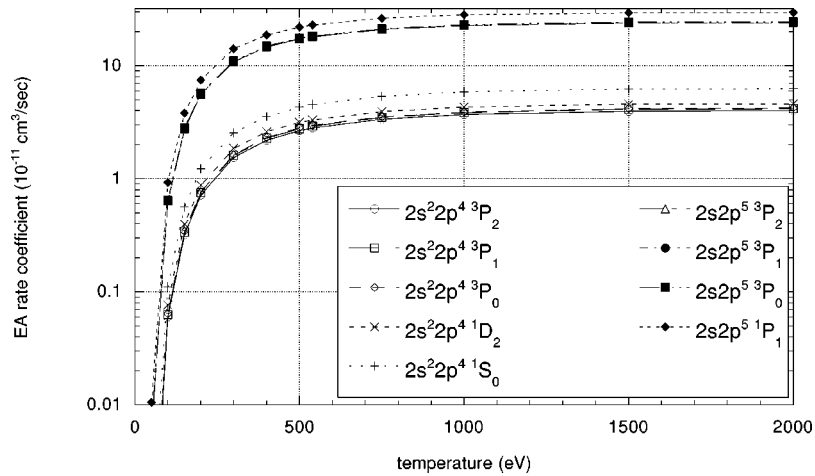


FIG. 3. EA rate coefficient for the O-like Ar^{10+} $2s^2 2p^4$ ($^3P_{2,1,0}$, 1D_2 , and 1S_0) ground and $2s2p^5$ (3P and 1P) excited energy levels.

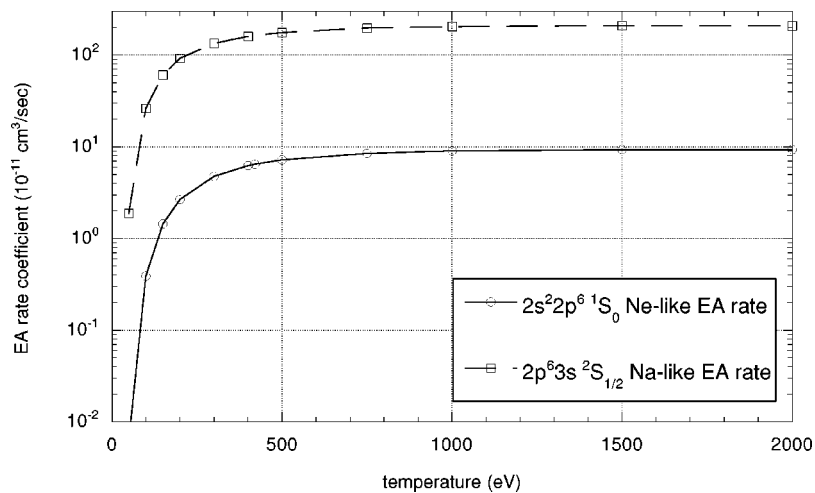


FIG. 4. EA rate coefficient for the Na-like Ar^{7+} $2s^2 2p^6 3s^2 \ ^2S_{1/2}$ ground level. Shown for comparison is the Ne-like Ar^{8+} $2s^2 2p^6 \ ^1S_0$ EA rate coefficient from Fig. 1.

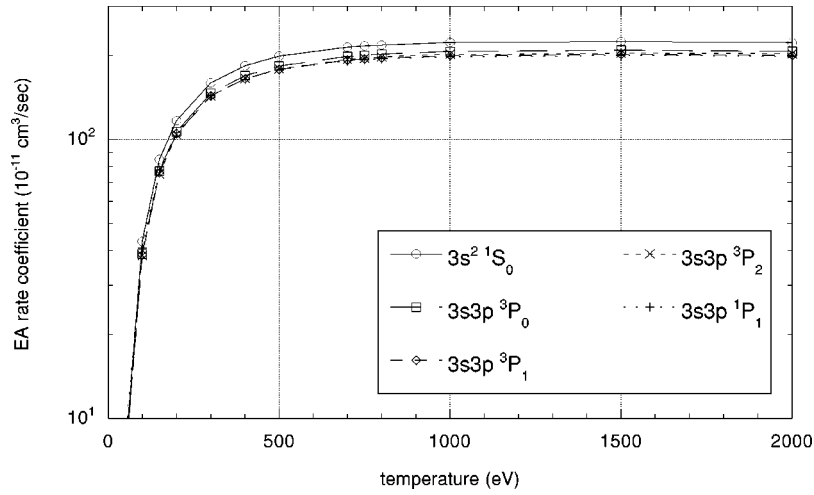


FIG. 5. EA rate coefficient for the Mg-like Ar^{6+} $2s^2 2p^6 3s^2 \ ^1S_0$ ground and $2s^2 2p^6 3s3p$ ($^3P_{0,1,2}$ and 1P_1) excited energy levels.

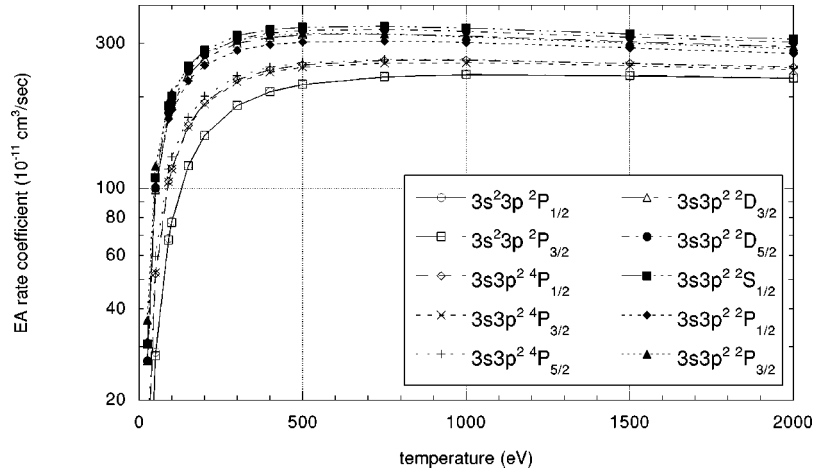


FIG. 6. EA rate coefficient for the Al-like Ar^{5+} $3s^2 3p$ ($^2P_{1/2}$ and $^2P_{3/2}$) ground and $3s3p^2$ (4P , 2D , 2S , and 2P) excited energy levels.

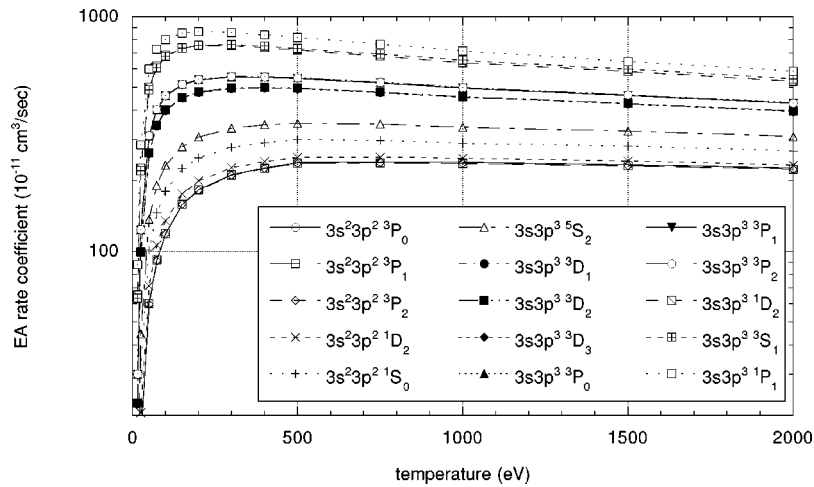


FIG. 7. EA rate coefficient for the Si-like Ar^{4+} $3s^2 3p^2$ ($^3P_{0,1,2}$, 1D_2 , and 1S_0) ground and $3s3p^3$ (5S , 3D , 3P , 1D , 3S , and 1P) excited energy levels.

coefficients increase with the increasing number of bound electrons; this simply reflects the increasing cross section for collisional excitation of a bound electron in the ground level of each ion with increasing occupancy. There is a marked difference in the shape of the rate coefficient for the Li- and Be-like ions and the remaining B- to Ne-like ions, particularly at low temperatures. The difference in the shape of the rate coefficients is due to the difference in characteristic excitation energies from the K -shell ($1s$ -electron) promotions in the case of Li- and Be-like ions and the L -shell ($2s$ -electron) promotions that dominate the EA process in the remaining ions.

The rate coefficients for EA from the ground and excited configurations of Be-like Ar^{14+} are shown in Fig. 2. The EA rate coefficients for the levels of the first excited configuration in Be-like Ar^{14+} are similar in shape to the rate coefficients for the ground levels in the B- to Ne-like ions (shown in Fig. 1); this is due to a contribution to the total EA rate coefficient from $2s$ -electron promotions in the levels of the first excited configuration that is absent in the EA rate coefficient of the ground level (see Table I). The EA rate coefficients in Fig. 2 for the 3P levels of the first excited configuration are nearly degenerate; this near degeneracy obtains for all the energy levels of a given LS term in every ion. The EA rate coefficients for the levels of the ground and first excited configuration in O-like Ar^{10+} are shown in Fig. 3. Again, as seen in Fig. 2, the EA rate coefficients in Fig. 3 for all three levels of the triplet terms ($2s^22p^4\ {}^3P$ and $2s2p^5\ {}^3P$) are nearly degenerate. For the levels of a given LS term, the radial parts of the impact excitation rate coefficients are the same [28] and only the angular factors are different. The Be- and O-like ions have been chosen as representative ions; the rate coefficients for EA from the ground and first excited configurations in all other L -shell ions look similar. The calculated rate coefficients for EA from the levels of the ground and first excited configuration in each L -shell argon ion are tabulated in Table III.

B. M -shell ions, Ar^{7+} to Ar^{2+}

The EA rate coefficients from the levels of the low-lying configurations in the Na- to Si-like M -shell argon ions are

shown in Figs. 4–7. For comparison, the L -shell Ne-like Ar^{8+} EA rate coefficient from Fig. 1 is plotted with the Na-like Ar^{7+} EA rate coefficient in Fig. 4. One sees that the M -shell ion's rate coefficient is more than an order of magnitude larger; the presence of a $3s$ electron in the Na-like ion means that the promotion of a $2p$ electron results in an autoionizing level, unlike the Ne-like ion, where only $2s$ promotions result in autoionizing levels (compare Tables II and I). As with the L -shell ions, the ground-level EA rate coefficient for the M -shell ions is seen to increase from Fig. 4 to Fig. 7 with increasing number of bound electrons. This trend continues in the ground level EA rates of P- and S-like Ar^{3+} and Ar^{2+} . The calculated rate coefficients for EA from the levels of the ground and first excited configuration in each M -shell argon ion are tabulated in Table III. As with the L -shell ions, one sees in Figs. 6 and 7 that the EA rate coefficients for different levels of a particular LS term in some configuration are nearly equal.

The convergence achieved in the calculation of the EA rate coefficient for the Na- and Mg-like argon ions can be seen in Fig. 8. The running sum of the L - ($2l \rightarrow n'l'$) and M -shell ($3s \rightarrow n'l'$ in the case of Mg-like Ar^{6+}) contributions to EA at each ion's ionization potential ($T_{\text{IP}} = 142$ and 121 eV for Na- and Mg-like argon, respectively) is plotted versus the principal quantum number. It is believed that the flatness of the running sums indicates that convergence has been achieved. The running sum of the contribution of two L -shell channels and one M -shell channel to the $2s^22p^63s^23p\ {}^2P$ ground levels in Al-like Ar^{5+} is shown in Fig. 9. The contribution of each manifold of levels is computed at the ion's ionization potential $T_{\text{IP}}=90$ eV. In the M -shell contribution ($3s^23p \rightarrow 3s3pn'l'$) to the ground levels' total EA rate coefficients, the sharp increase in the running sum from $n'=6$ to $n'=7$ is due to the fact that for $n'=5$ and 6, the majority of the levels of the $3s3pn'l'$ configurations are below the continuum of the Al-like ion. When $n'=7$, all the levels of the $3s3p7l'$ configurations are above the continuum and can contribute to the EA process. Clearly, in the case of Al-like argon the M -shell contribution dominates the total EA rate coefficient.

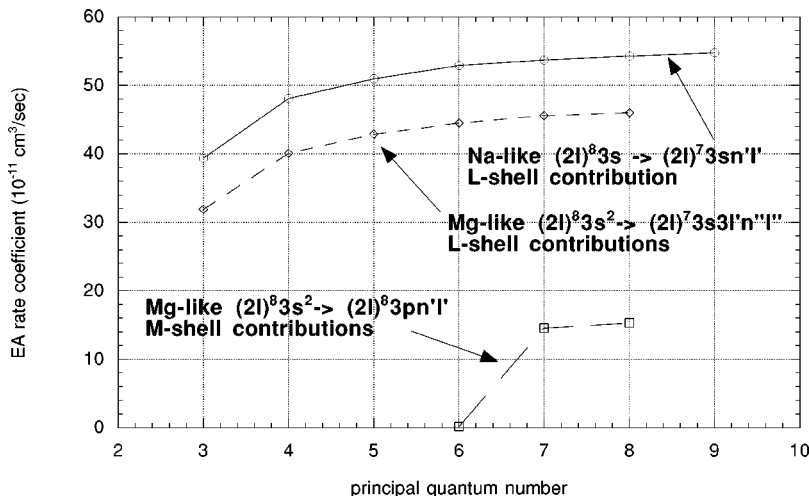


FIG. 8. Running sum of the contribution of $2s$ and $2p$ (L -shell) excitations to the total EA rate coefficient of the ground levels in Na- and Mg-like argon ions. Also shown is the running sum of the contribution of $3s$ (M -shell) excitations to the total EA rate for the ground level in Mg-like argon.

TABLE III. EA rate coefficients for the levels of the ground and first excited configurations in Ar^{15+} to Ar^{2+} . The rate coefficients are given in units of $10^{-11} \text{ cm}^3 \text{ sec}^{-1}$. Numbers in square brackets represent powers of 10, i.e., $X[-Y]=X \times 10^{-Y}$.

Li-like Ar^{15+}			
T_e (eV)	$1s^2 2s^2 \ ^2S_{1/2}$	$1s^2 2p^2 \ ^2P_{1/2}$	$1s^2 2p^2 \ ^2P_{3/2}$
200.0	3.36[-7]	4.15[-7]	4.35[-7]
300.0	4.98[-5]	6.07[-5]	6.44[-5]
400.0	5.89[-4]	7.14[-4]	7.59[-4]
500.0	2.55[-3]	3.08[-3]	3.28[-3]
750.0	1.74[-2]	2.09[-2]	2.23[-2]
918.0	3.44[-2]	4.16[-2]	4.47[-2]
1000.0	4.42[-2]	5.32[-2]	5.68[-2]
1500.0	1.08[-1]	1.31[-1]	1.40[-1]
2000.0	1.65[-1]	2.01[-1]	2.13[-1]
3100.0	2.50[-1]	3.11[-1]	3.27[-1]
4000.0	2.91[-1]	3.67[-1]	3.84[-1]

Be-like Ar^{14+}					
T_e (eV)	$1s^2 2s^2 \ ^1S_0$	$1s^2 2s 2p \ ^3P_0$	$1s^2 2s 2p \ ^3P_1$	$1s^2 2s 2p \ ^3P_2$	$1s^2 2s 2p \ ^1P_1$
200.0	7.65[-7]	1.31[-2]	1.31[-2]	1.30[-2]	1.54[-2]
300.0	1.12[-4]	4.22[-2]	4.21[-2]	4.19[-2]	4.71[-2]
400.0	1.33[-3]	7.38[-2]	7.37[-2]	7.33[-2]	8.06[-2]
500.0	5.79[-3]	1.04[-1]	1.04[-1]	1.03[-1]	1.12[-1]
750.0	4.00[-2]	1.76[-1]	1.75[-1]	1.74[-1]	1.88[-1]
850.0	6.23[-2]	2.07[-1]	2.05[-1]	2.04[-1]	2.21[-1]
1000.0	1.02[-1]	2.51[-1]	2.48[-1]	2.47[-1]	2.70[-1]
1500.0	2.53[-1]	3.97[-1]	3.87[-1]	3.85[-1]	4.29[-1]
2000.0	3.89[-1]	5.19[-1]	5.01[-1]	4.97[-1]	5.62[-1]
3000.0	5.82[-1]	6.87[-1]	6.55[-1]	6.47[-1]	7.41[-1]

B-like Ar^{13+}					
T_e (eV)	$2s^2 2p^2 \ ^2P_{1/2}$	$2s^2 2p^2 \ ^2P_{3/2}$	$2s 2p^2 \ ^4P_{1/2}$	$2s 2p^2 \ ^4P_{3/2}$	$2s 2p^2 \ ^4P_{5/2}$
110.0	1.32[-3]	1.48[-3]	3.42[-3]	3.37[-3]	3.49[-3]
150.0	7.27[-3]	8.15[-3]	1.83[-2]	1.81[-2]	1.87[-2]
200.0	2.30[-2]	2.59[-2]	5.70[-2]	5.63[-2]	5.80[-2]
300.0	6.71[-2]	7.60[-2]	1.63[-1]	1.61[-1]	1.65[-1]
400.0	1.13[-1]	1.28[-1]	2.68[-1]	2.64[-1]	2.70[-1]
500.0	1.53[-1]	1.74[-1]	3.55[-1]	3.50[-1]	3.56[-1]
750.0	2.43[-1]	2.72[-1]	5.01[-1]	4.94[-1]	5.00[-1]
756.0	2.45[-1]	2.75[-1]	5.04[-1]	4.97[-1]	5.03[-1]
1000.0	3.23[-1]	3.56[-1]	5.84[-1]	5.75[-1]	5.80[-1]
1500.0	4.65[-1]	4.99[-1]	6.65[-1]	6.57[-1]	6.58[-1]
2000.0	5.78[-1]	6.09[-1]	7.03[-1]	6.95[-1]	6.93[-1]
3000.0	7.26[-1]	7.51[-1]	7.28[-1]	7.22[-1]	7.16[-1]

T_e (eV)	$2s 2p^2 \ ^2D_{3/2}$	$2s 2p^2 \ ^2D_{5/2}$	$2s 2p^2 \ ^2S_{1/2}$	$2s 2p^2 \ ^2P_{1/2}$	$2s 2p^2 \ ^2P_{3/2}$
110.0	1.01[-2]	1.00[-2]	1.06[-2]	1.11[-2]	1.23[-2]
150.0	5.06[-2]	5.02[-2]	5.23[-2]	5.33[-2]	5.85[-2]
200.0	1.50[-1]	1.49[-1]	1.54[-1]	1.53[-1]	1.67[-1]
300.0	4.07[-1]	4.07[-1]	4.16[-1]	4.02[-1]	4.38[-1]
400.0	6.53[-1]	6.54[-1]	6.67[-1]	6.32[-1]	6.89[-1]
500.0	8.50[-1]	8.53[-1]	8.68[-1]	8.11[-1]	8.85[-1]
750.0	1.17	1.17	1.20	1.09	1.19
756.0	1.17	1.18	1.20	1.09	1.20
1000.0	1.34	1.35	1.37	1.23	1.35

TABLE III. (Continued).

Be-like Ar ¹³⁺					
T_e (eV)	$2s2p^2\ ^2D_{3/2}$	$2s2p^2\ ^2D_{5/2}$	$2s2p^2\ ^2S_{1/2}$	$2s2p^2\ ^2P_{1/2}$	$2s2p^2\ ^2P_{3/2}$
1500.0	1.48	1.50	1.53	1.34	1.47
2000.0	1.53	1.55	1.59	1.38	1.52
3000.0	1.55	1.57	1.62	1.38	1.52
C-like Ar ¹²⁺					
T_e (eV)	$2s^22p^2\ ^3P_0$	$2s^22p^2\ ^3P_1$	$2s^22p^2\ ^3P_2$	$2s^22p^2\ ^2D_2$	$2s^22p^2\ ^1S_0$
50.0	4.60[-6]	4.88[-6]	5.41[-6]	9.97[-6]	1.47[-5]
100.0	3.48[-3]	3.68[-3]	4.01[-3]	6.57[-3]	9.27[-3]
150.0	2.93[-2]	3.09[-2]	3.36[-2]	5.27[-2]	7.33[-2]
200.0	8.17[-2]	8.63[-2]	9.35[-2]	1.44[-1]	1.99[-1]
300.0	2.16[-1]	2.29[-1]	2.47[-1]	3.70[-1]	5.08[-1]
400.0	3.39[-1]	3.59[-1]	3.88[-1]	5.72[-1]	7.84[-1]
500.0	4.40[-1]	4.66[-1]	5.05[-1]	7.37[-1]	1.01
686.0	5.65[-1]	6.00[-1]	6.52[-1]	9.40[-1]	1.28
750.0	5.94[-1]	6.31[-1]	6.85[-1]	9.86[-1]	1.34
1000.0	6.76[-1]	7.19[-1]	7.83[-1]	1.12	1.52
1500.0	7.43[-1]	7.94[-1]	8.68[-1]	1.23	1.66
2000.0	7.65[-1]	8.18[-1]	8.97[-1]	1.26	1.70
3000.0	7.64[-1]	8.19[-1]	9.04[-1]	1.26	1.70
T_e (eV)	$2s2p^3\ ^5S_2$	$2s2p^3\ ^3D_1$	$2s2p^3\ ^3D_2$	$2s2p^3\ ^3D_3$	$2s2p^3\ ^3P_0$
50.0	9.11[-6]	5.83[-5]	6.06[-5]	5.40[-5]	7.46[-5]
100.0	6.09[-3]	2.74[-2]	2.83[-2]	2.55[-2]	3.31[-2]
150.0	4.90[-2]	1.97[-1]	2.03[-1]	1.84[-1]	2.34[-1]
200.0	1.34[-1]	5.10[-1]	5.23[-1]	4.73[-1]	5.98[-1]
300.0	3.44[-1]	1.25	1.28	1.16	1.45
400.0	5.30[-1]	1.89	1.93	1.75	2.19
500.0	6.80[-1]	2.39	2.44	2.21	2.75
686.0	8.58[-1]	3.01	3.05	2.76	3.44
750.0	8.99[-1]	3.15	3.20	2.89	3.60
1000.0	1.01	3.78	3.80	3.53	4.35
1500.0	1.09	4.13	4.14	3.84	4.73
2000.0	1.11	4.25	4.25	3.95	4.85
3000.0	1.10	4.25	4.25	3.94	4.83
T_e (eV)	$2s2p^3\ ^3P_1$	$2s2p^3\ ^3P_2$	$2s2p^3\ ^1D_2$	$2s2p^3\ ^3S_1$	$2s2p^3\ ^1P_1$
50.0	7.23[-5]	6.84[-5]	1.56[-4]	1.71[-4]	2.07[-4]
100.0	3.22[-2]	3.07[-2]	5.61[-2]	6.03[-2]	6.88[-2]
150.0	2.27[-1]	2.18[-1]	3.68[-1]	3.94[-1]	4.40[-1]
200.0	5.81[-1]	5.58[-1]	9.04[-1]	9.65[-1]	1.07
300.0	1.41	1.36	2.11	2.24	2.46
400.0	2.12	2.04	3.11	3.30	3.60
500.0	2.67	2.57	3.86	4.10	4.46
686.0	3.34	3.21	4.75	5.03	5.47
750.0	3.49	3.36	4.97	5.25	5.71
1000.0	4.19	4.04	5.94	6.35	6.84
1500.0	4.55	4.39	6.40	6.84	7.34
2000.0	4.66	4.50	6.53	6.96	7.47
3000.0	4.64	4.47	6.49	6.90	7.40

TABLE III. (Continued).

N-like Ar ¹¹⁺					
T_e (eV)	$2s^22p^3\ ^4S_{3/2}$	$2s^22p^3\ ^2D_{3/2}$	$2s^22p^3\ ^2D_{5/2}$	$2s^22p^3\ ^2P_{1/2}$	$2s^22p^3\ ^2P_{3/2}$
50.0	2.12[-5]	4.61[-5]	4.69[-5]	9.77[-5]	9.83[-5]
100.0	9.36[-3]	1.73[-2]	1.76[-2]	3.22[-2]	3.24[-2]
150.0	6.59[-2]	1.15[-1]	1.17[-1]	2.05[-1]	2.06[-1]
200.0	1.69[-1]	2.84[-1]	2.89[-1]	5.00[-1]	5.02[-1]
300.0	4.12[-1]	6.69[-1]	6.80[-1]	1.16	1.16
400.0	6.25[-1]	9.95[-1]	1.01	1.70	1.71
500.0	7.91[-1]	1.24	1.26	2.12	2.13
619.0	9.36[-1]	1.46	1.48	2.47	2.48
750.0	1.05	1.62	1.64	2.73	2.75
1000.0	1.18	1.80	1.83	3.04	3.06
1500.0	1.29	1.96	1.99	3.28	3.30
2000.0	1.33	2.00	2.03	3.34	3.37
3000.0	1.33	1.99	2.02	3.31	3.34
T_e (eV)	$2s2p^4\ ^4P_{5/2}$	$2s2p^4\ ^4P_{3/2}$	$2s2p^4\ ^4P_{1/2}$	$2s2p^4\ ^2P_{3/2}$	$2s2p^4\ ^2D_{5/2}$
50.0	3.84[-4]	4.12[-4]	4.34[-4]	8.13[-4]	8.30[-4]
100.0	9.50[-2]	1.00[-1]	1.05[-1]	1.64[-1]	1.66[-1]
150.0	5.53[-1]	5.80[-1]	6.03[-1]	8.87[-1]	9.01[-1]
200.0	1.28	1.34	1.39	1.99	2.02
300.0	2.83	2.96	3.06	4.23	4.30
400.0	4.08	4.26	4.41	6.00	6.08
500.0	4.99	5.21	5.39	7.25	7.35
619.0	5.75	6.01	6.21	8.28	8.40
750.0	6.33	6.61	6.83	9.05	9.17
1000.0	6.98	7.28	7.52	9.87	1.00
1500.0	7.46	7.79	8.05	1.05	1.06
2000.0	7.58	7.92	8.18	1.06	1.07
3000.0	7.52	7.88	8.13	1.05	1.06
T_e (eV)	$2s2p^4\ ^2P_{1/2}$	$2s2p^4\ ^2D_{3/2}$	$2s2p^4\ ^2S_{1/2}$		
50.0	1.52[-3]	1.25[-3]	1.44[-3]		
100.0	2.62[-1]	2.25[-1]	2.50[-1]		
150.0	1.35	1.17	1.29		
200.0	2.95	2.57	2.82		
300.0	6.15	5.37	5.86		
400.0	8.62	7.54	8.21		
500.0	1.04[1]	9.06	9.85		
619.0	1.18[1]	1.03[1]	1.12[1]		
750.0	1.28[1]	1.12[1]	1.22[1]		
1000.0	1.40[1]	1.22[1]	1.33[1]		
1500.0	1.48[1]	1.29[1]	1.41[1]		
2000.0	1.50[1]	1.30[1]	1.42[1]		
3000.0	1.48[1]	1.29[1]	1.40[1]		
O-like Ar ¹⁰⁺					
T_e (eV)	$2s^22p^4\ ^3P_2$	$2s^22p^4\ ^3P_1$	$2s^22p^4\ ^3P_0$	$2s^22p^4\ ^2D_2$	$2s^22p^4\ ^1S_0$
50.0	3.07[-4]	3.27[-4]	3.35[-4]	4.25[-4]	6.76[-4]
100.0	6.00[-2]	6.31[-2]	6.43[-2]	7.65[-2]	1.11[-1]
150.0	3.23[-1]	3.38[-1]	3.44[-1]	4.00[-1]	5.63[-1]
200.0	7.22[-1]	7.55[-1]	7.67[-1]	8.82[-1]	1.22
300.0	1.55	1.61	1.63	1.86	2.55
400.0	2.20	2.29	2.32	2.61	3.57
500.0	2.67	2.78	2.82	3.16	4.32

TABLE III. (Continued).

O-like Ar ¹⁰⁺					
T_e (eV)	$2s^22p^4\ ^3P_2$	$2s^22p^4\ ^3P_1$	$2s^22p^4\ ^3P_0$	$2s^22p^4\ ^2D_2$	$2s^22p^4\ ^1S_0$
538.0	2.82	2.93	2.97	3.33	4.53
750.0	3.37	3.50	3.55	3.94	5.37
1000.0	3.71	3.85	3.90	4.30	5.87
1500.0	3.97	4.12	4.18	4.56	6.24
2000.0	4.03	4.10	4.24	4.60	6.32
3000.0	3.98	4.14	4.19	4.50	6.22
T_e (eV)	$2s2p^5\ ^3P_2$	$2s2p^5\ ^3P_1$	$2s2p^5\ ^3P_0$	$2s2p^5\ ^1P_1$	
50.0	6.11[-3]	6.20[-3]	6.24[-3]	1.06[-2]	
100.0	6.36[-1]	6.40[-1]	6.45[-1]	9.28[-1]	
150.0	2.78	2.79	2.82	3.83	
200.0	5.61	5.63	5.69	7.51	
300.0	1.09[1]	1.09[1]	1.10[1]	1.41[1]	
400.0	1.47[1]	1.47[1]	1.49[1]	1.88[1]	
500.0	1.73[1]	1.73[1]	1.76[1]	2.20[1]	
538.0	1.81[1]	1.81[1]	1.84[1]	2.29[1]	
750.0	2.10[1]	2.10[1]	2.13[1]	2.63[1]	
1000.0	2.27[1]	2.27[1]	2.30[1]	2.82[1]	
1500.0	2.39[1]	2.39[1]	2.43[1]	2.95[1]	
2000.0	2.41[1]	2.41[1]	2.45[1]	2.97[1]	
3000.0	2.38[1]	2.37[1]	2.42[1]	2.92[1]	
F-like Ar ⁹⁺			Ne-like Ar ⁸⁺		
T_e (eV)	$2s^22p^5\ ^2P_{3/2}$	$2s^22p^5\ ^2P_{1/2}$	$2s2p^6\ ^2S_{1/2}$	T_e (eV)	$2s^22p^6\ ^1S_0$
50.0	1.64[-3]	1.76[-3]	4.42[-2]	50.0	6.32[-3]
100.0	1.74[-1]	1.84[-1]	2.28	100.0	3.89[-1]
150.0	7.67[-1]	8.07[-1]	7.93	150.0	1.43
200.0	1.56	1.63	1.43[1]	200.0	2.67
300.0	3.06	3.20	2.50[1]	300.0	4.76
400.0	4.15	4.33	3.21[1]	400.0	6.21
478.0	4.76	4.97	3.60[1]	421.0	6.44
500.0	4.91	5.12	3.68[1]	500.0	7.18
750.0	5.99	6.24	4.33[1]	750.0	8.47
1000.0	6.46	6.73	4.61[1]	1000.0	9.02
1500.0	6.79	7.07	4.80[1]	1500.0	9.31
2000.0	6.84	7.11	4.83[1]	2000.0	9.27
3000.0	6.69	6.96	4.72[1]		
Na-like Ar ⁷⁺					
T_e (eV)	$2p^63s\ ^2S_{1/2}$				
50.0	1.88				
100.0	2.62[1]				
142.0	5.57[1]				
150.0	6.10[1]				
200.0	9.16[1]				
300.0	1.34[2]				
400.0	1.60[2]				
500.0	1.76[2]				
750.0	1.97[2]				
1000.0	2.05[2]				
1500.0	2.09[2]				
2000.0	2.08[2]				

TABLE III. (Continued).

Mg-like Ar ⁶⁺					
T_e (eV)	$3s^2\ ^1S_0$	$3s3p\ ^3P_0$	$3s3p\ ^3P_1$	$3s3p\ ^3P_2$	$3s3p\ ^1P_1$
50.0	7.28	6.87	6.92	7.06	8.48
100.0	4.31[1]	3.88[1]	3.86[1]	3.84[1]	4.07[1]
121.0	6.13[1]	5.55[1]	5.49[1]	5.45[1]	5.70[1]
150.0	8.47[1]	7.70[1]	7.58[1]	7.54[1]	7.77[1]
200.0	1.17[2]	1.07[2]	1.05[2]	1.05[2]	1.06[2]
300.0	1.60[2]	1.46[2]	1.43[2]	1.43[2]	1.43[2]
400.0	1.84[2]	1.69[2]	1.65[2]	1.65[2]	1.65[2]
500.0	1.99[2]	1.83[2]	1.78[2]	1.79[2]	1.78[2]
750.0	2.16[2]	2.00[2]	1.94[2]	1.96[2]	1.93[2]
1000.0	2.22[2]	2.07[2]	2.00[2]	2.02[2]	1.98[2]
1500.0	2.24[2]	2.09[2]	2.02[2]	2.04[2]	2.00[2]
2000.0	2.22[2]	2.07[2]	2.00[2]	2.03[2]	1.98[2]
Al-like Ar ⁵⁺					
T_e (eV)	$3s^23p\ ^2P_{1/2}$	$3s^23p\ ^2P_{3/2}$	$3s3p^2\ ^4P_{1/2}$	$3s3p^2\ ^4P_{3/2}$	$3s3p^2\ ^4P_{5/2}$
10.0	2.40[-2]	2.29[-2]			
25.0	5.57	5.33	1.21[1]	1.24[1]	1.41[1]
50.0	2.88[1]	2.80[1]	5.22[1]	5.27[1]	5.95[1]
90.0	6.83[1]	6.74[1]	1.05[2]	1.05[2]	1.15[2]
100.0	7.78[1]	7.70[1]	1.16[2]	1.16[2]	1.27[2]
150.0	1.19[2]	1.18[2]	1.61[2]	1.59[2]	1.71[2]
200.0	1.50[2]	1.49[2]	1.92[2]	1.89[2]	2.01[2]
300.0	1.87[2]	1.87[2]	2.28[2]	2.24[2]	2.34[2]
400.0	2.08[2]	2.08[2]	2.45[2]	2.41[2]	2.50[2]
500.0	2.19[2]	2.20[2]	2.55[2]	2.50[2]	2.59[2]
750.0	2.32[2]	2.33[2]	2.64[2]	2.59[2]	2.65[2]
1000.0	2.36[2]	2.37[2]	2.64[2]	2.59[2]	2.64[2]
1500.0	2.34[2]	2.35[2]	2.58[2]	2.53[2]	2.57[2]
2000.0	2.30[2]	2.30[2]	2.50[2]	2.45[2]	2.48[2]
Al-like Ar ⁵⁺					
T_e (eV)	$3s3p\ ^2D_{3/2}$	$3s3p^2\ ^2D_{5/2}$	$3s3p^2\ ^2S_{1/2}$	$3s3p^2\ ^2P_{1/2}$	$3s3p^2\ ^2P_{3/2}$
10.0					
25.0	2.70[1]	2.70[1]	3.06[1]	3.11[1]	3.67[1]
50.0	9.89[1]	1.00[2]	1.08[2]	1.02[2]	1.18[2]
90.0	1.74[2]	1.77[2]	1.87[2]	1.69[2]	1.93[2]
100.0	1.87[2]	1.91[2]	2.01[2]	1.81[2]	2.06[2]
150.0	2.37[2]	2.43[2]	2.53[2]	2.26[2]	2.52[2]
200.0	2.68[2]	2.75[2]	2.85[2]	2.54[2]	2.79[2]
300.0	3.00[2]	3.10[2]	3.19[2]	2.84[2]	3.07[2]
400.0	3.14[2]	3.25[2]	3.33[2]	2.97[2]	3.19[2]
500.0	3.20[2]	3.31[2]	3.39[2]	3.03[2]	3.23[2]
750.0	3.22[2]	3.33[2]	3.41[2]	3.05[2]	3.22[2]
1000.0	3.18[2]	3.29[2]	3.37[2]	3.01[2]	3.16[2]
1500.0	3.04[2]	3.15[2]	3.22[2]	2.89[2]	3.00[2]
2000.0	2.92[2]	3.02[2]	3.09[2]	2.77[2]	2.87[2]
Si-like Ar ⁴⁺					
T_e (eV)	$3s^23p^2\ ^3P_0$	$3s^23p^2\ ^3P_1$	$3s^23p^2\ ^3P_2$	$3s^23p^2\ ^1D_2$	$3s^23p^2\ ^1S_0$
25.0	1.66[1]	1.66[1]	1.64[1]	2.05[1]	3.07[1]
50.0	6.01[1]	6.02[1]	5.97[1]	7.14[1]	1.01[2]
74.0	9.17[1]	9.19[1]	9.13[1]	1.06[2]	1.46[2]
100.0	1.19[2]	1.19[2]	1.19[2]	1.35[2]	1.80[2]
150.0	1.59[2]	1.59[2]	1.58[2]	1.76[2]	2.25[2]
200.0	1.83[2]	1.83[2]	1.83[2]	2.00[2]	2.50[2]
300.0	2.13[2]	2.12[2]	2.11[2]	2.28[2]	2.78[2]
400.0	2.27[2]	2.26[2]	2.25[2]	2.41[2]	2.90[2]
500.0	2.39[2]	2.38[2]	2.37[2]	2.52[2]	3.00[2]
750.0	2.41[2]	2.39[2]	2.38[2]	2.52[2]	29.7[2]

TABLE III. (Continued).

Si-like Ar ⁴⁺					
T_e (eV)	$3s^23p^2\ ^3P_0$	$3s^23p^2\ ^3P_1$	$3s^23p^2\ ^3P_2$	$3s^23p^2\ ^1D_2$	$3s^23p^2\ ^1S_0$
1000.0	2.40[2]	2.37[2]	2.37[2]	2.49[2]	2.89[2]
1500.0	2.34[2]	2.31[2]	2.32[2]	2.42[2]	2.81[2]
2000.0	2.26[2]	2.24[2]	2.24[2]	2.33[2]	2.68[2]
T_e (eV)	$3s3p^3\ ^5S_2$	$3s3p^3\ ^3D_1$	$3s3p^3\ ^3D_2$	$3s3p^3\ ^3D_3$	$3s3p^3\ ^3P_0$
15.0	8.04	2.25[1]	2.26[1]	2.24[1]	3.00[1]
25.0	4.46[1]	9.90[1]	9.95[1]	9.87[1]	1.24[2]
50.0	1.37[2]	2.62[2]	2.63[2]	2.61[2]	3.11[2]
74.0	1.91[2]	3.43[2]	3.45[2]	3.42[2]	4.02[2]
100.0	2.33[2]	3.99[2]	4.00[2]	3.97[2]	4.61[2]
150.0	2.79[2]	4.51[2]	4.53[2]	4.50[2]	5.15[2]
200.0	3.08[2]	4.77[2]	4.79[2]	4.75[2]	5.40[2]
300.0	3.35[2]	4.96[2]	4.98[2]	4.94[2]	5.56[2]
400.0	3.47[2]	4.98[2]	5.00[2]	4.97[2]	5.55[2]
500.0	3.51[2]	4.94[2]	4.96[2]	4.93[2]	5.48[2]
750.0	3.49[2]	4.77[2]	4.79[2]	4.76[2]	5.26[2]
1000.0	3.38[2]	4.55[2]	4.56[2]	4.54[2]	4.99[2]
1500.0	3.26[2]	4.26[2]	4.27[2]	4.25[2]	4.65[2]
2000.0	3.08[2]	3.95[2]	3.96[2]	3.94[2]	4.29[2]
Si-like Ar ⁴⁺					
T_e (eV)	$3s3p^3\ ^3P_1$	$3s3p^3\ ^3P_2$	$3s3p^3\ ^1D_2$	$3s3p^3\ ^3S_1$	$3s3p^3\ ^1P_1$
15.0	2.99[1]	3.01[1]	6.54[1]	6.33[1]	8.79[1]
25.0	1.23[2]	1.24[2]	2.26[2]	2.21[2]	2.84[2]
50.0	3.10[2]	3.12[2]	5.00[2]	4.88[2]	5.98[2]
74.0	4.00[2]	4.03[2]	6.17[2]	6.06[2]	7.26[2]
100.0	4.59[2]	4.62[2]	6.85[2]	6.78[2]	7.99[2]
150.0	5.13[2]	5.16[2]	7.37[2]	7.35[2]	8.50[2]
200.0	5.38[2]	5.41[2]	7.55[2]	7.57[2]	8.64[2]
300.0	5.53[2]	5.56[2]	7.54[2]	7.61[2]	8.57[2]
400.0	5.52[2]	5.55[2]	7.40[2]	7.49[2]	8.37[2]
500.0	5.45[2]	5.49[2]	7.22[2]	7.34[2]	8.15[2]
750.0	5.23[2]	5.26[2]	6.79[2]	6.93[2]	7.63[2]
1000.0	4.97[2]	4.99[2]	6.38[2]	6.52[2]	7.15[2]
1500.0	4.62[2]	4.65[2]	5.85[2]	5.98[2]	6.44[2]
2000.0	4.27[2]	4.29[2]	5.31[2]	5.43[2]	5.85[2]
P-like Ar ³⁺					
T_e (eV)	$3s^23p^3\ ^4S_{3/2}$	$3s^23p^3\ ^2D_{3/2}$	$3s^23p^3\ ^2D_{5/2}$	$3s^23p^3\ ^2P_{1/2}$	$3s^23p^3\ ^2P_{3/2}$
10.0	1.53	3.28	3.40	5.19	5.11
15.0	1.01[1]	1.93[1]	2.00[1]	2.85[1]	2.81[1]
20.0	2.53[1]	4.53[1]	4.73[1]	6.51[1]	6.39[1]
25.0	4.31[1]	7.42[1]	7.76[1]	1.05[2]	1.03[2]
50.0	1.15[2]	1.81[2]	1.90[2]	2.47[2]	2.42[2]
57.0	1.26[2]	1.97[2]	2.08[2]	2.70[2]	2.63[2]
100.0	1.74[2]	2.54[2]	2.66[2]	3.42[2]	3.32[2]
150.0	1.95[2]	2.74[2]	2.86[2]	3.66[2]	3.53[2]
200.0	2.04[2]	2.79[2]	2.91[2]	3.70[2]	3.56[2]
300.0	2.08[2]	2.75[2]	2.87[2]	3.64[2]	3.46[2]
400.0	2.07[2]	2.67[2]	2.80[2]	3.53[2]	3.34[2]

TABLE III. (Continued).

T_e (eV)	S-like Ar^{2+}				
	$3s^23p^4\ ^3P_2$	$3s^23p^4\ ^3P_1$	$3s^23p^4\ ^3P_0$	$3s^23p^4\ ^1D_2$	$3s^23p^4\ ^1S_0$
5.0	5.78[-1]	6.11[-1]	6.25[-1]	1.15	2.95
10.0	3.47[1]	3.64[1]	3.69[1]	5.48[1]	1.06[2]
15.0	1.29[2]	1.36[2]	1.37[2]	1.89[2]	3.33[2]
20.0	2.43[2]	2.55[2]	2.57[2]	3.40[2]	5.74[2]
30.0	4.41[2]	4.60[2]	4.64[2]	5.90[2]	9.49[2]
40.0	5.77[2]	6.02[2]	6.06[2]	7.55[2]	1.19[3]
41.0	5.72[2]	5.97[2]	6.01[2]	7.49[2]	1.17[3]
50.0	6.52[2]	6.81[2]	6.84[2]	8.42[2]	1.30[3]
100.0	8.18[2]	8.55[2]	8.58[2]	1.02[3]	1.54[3]
150.0	8.38[2]	8.78[2]	8.80[2]	1.03[3]	1.53[3]
200.0	8.24[2]	8.65[2]	8.67[2]	1.00[3]	1.49[3]
300.0	7.84[2]	8.24[2]	8.25[2]	9.42[2]	1.39[3]

The total rate coefficient for EA has been calculated for the levels of the ground configuration in the P-like Ar^{3+} and S-like Ar^{2+} ions with the formalism described above. The RELAC code is highly accurate for calculation of the energy-level structure in highly ionized, heavy elements [31]. The accuracy of the code increases with increasing importance of relativistic effects on the ionic structure and with the increasing depth of the ionic potential. It is believed that the S-like Ar^{2+} ion is the limit of ions that can be treated accurately with RELAC. The EA rate coefficients from the levels of the ground configuration in P-like Ar^{3+} and S-like Ar^{2+} are reported in Table III. Figure 10 shows the total EA rate coefficient for each argon ion in the present work computed at an electron temperature equal to the first ionization energy in each ion. The EA rate coefficients from the ground levels in Cl-like Ar^{1+} have been computed for Fig. 10, but are not reported in Table III. The regularity of the increase of the ground level EA rate coefficient and the similarity in the pattern of the L -shell ions' rates and the M -shell ions' rates with increasing number of valence electrons seen in Fig. 10 are evidence of the validity of RELAC's wave-function calculations for the Ar^{3+} and Ar^{2+} ions.

While from Eq. (1) one sees that only energy levels in the continuum formed by a single excitation contribute to the EA process, our multiconfiguration atomic structure calculations enable contributions to EA from doubly and triply excited states. For Na-like Ar^{7+} , all possible doubly excited configurations in the $n=3$ manifold of levels have been included in our calculations [e.g., configurations of the form $(2l)^73p^2$, $(2l)^73p3d$, and $(2l)^73d^2$, $l=s,p$]; due to wavefunction mixing, levels from these configurations contribute about 11% to the total L -shell EA rate coefficient through the $n=3$ manifold of levels. For Mg-like Ar^{6+} , doubly and triply excited states in the $n=3$ manifold of levels have been included in the calculation of the EA rate coefficient [that is, the $(2l)^73s3p^2$, $(2l)^73s3p3d$, $(2l)^73s3d^2$, and $(2l)^73p^3$ configurations have been considered]. Wavefunction mixing allows these multiply excited states to contribute $\approx 30\%$ of the total EA rate coefficient through the L -shell excitations in the $n=3$ manifold of levels. Since the EA rate coefficient for the four levels of the $3s3p$ (3P and 1P) configuration in Ar^{6+} have also been computed, excited states of the form $(2l)^73s3pn'l'$ and $(2l)^83pn'l'$ have been included in our

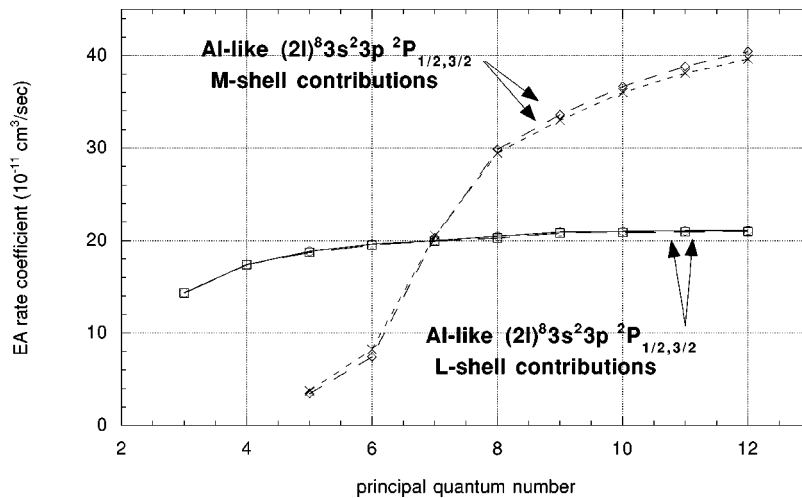


FIG. 9. Running sum of the contribution of the $(2l)^83s^23p \rightarrow (2l)^73s^23pn'l'$ (L -shell) excitation channel to the total EA rate coefficient for the $3s^2\ ^2P_{1/2,3/2}$ levels in Al-like Ar^{5+} . Also shown is the M -shell contribution to EA through the $(2l)^83s^23p \rightarrow (2l)^83s3pn'l'$ channel.

models; these states are formed by the promotion of a $2l$ or $3s$ electron from the $(2l)^8 3s 3p$ configuration. Even though the above excited configurations cannot be reached by a single excitation from the ground level, it is found that the $(2l)^7 3s 3p n' l'$ and $(2l)^8 3p n' l'$ configurations are able to contribute (a small amount) to EA from the ground level because of wave-function mixing.

C. Radiative decays between continuum levels

The second term in the autoionization branching ratio in Eq. (2) represents autoionization following radiative transitions between energy levels in the continuum and thus represents an enhancement of the total EA cross section. It is found that radiative decays from a continuum energy level j to all other continuum levels,

$$\sum_{j'} A_{jj'}^R = \Gamma_j^{\text{rad}} - \Gamma_j^{\text{stab}}, \quad (17)$$

where Γ_j^{stab} represents a sum of radiative transition rates from level j in the continuum of ion Z to all levels f' below the continuum

$$\Gamma_j^{\text{stab}} = \sum_{f'} A_{jf'}^R, \quad (18)$$

is a small fraction of the total radiative width Γ_j^{rad} from that level

$$(\Gamma_j^{\text{rad}} - \Gamma_j^{\text{stab}}) / \Gamma_j^{\text{rad}} \leq 0.001. \quad (19)$$

Thus the enhancement of the EA rates for the argon ions in the present work due to transitions between energy levels in the continuum is small.

D. Comparison with other calculations

The autoionization branching ratios of the argon ions in the present work are sensitive to configuration interaction (CI). That is, when performing the calculations for the EA rate from a given level of an argon ion, the branching ratio for autoionization from a given intermediate (continuum) level can change by an order of magnitude depending on what type of wave-function mixing with other intermediate (continuum) energy levels is allowed. Chen [34] reached this conclusion nearly a decade ago. More recently, Teng and Xu [17] have demonstrated the effects of CI on the branching ratios of autoionizing levels in Na-like Ar^{7+} . Differences in the methods of calculation in Refs. [34] and [17] (multiconfiguration Dirac-Fock with Breit interaction versus Hartree-Fock with relativistic corrections, respectively) result in large differences in the branching ratios for autoionization from the Na-like energy levels. Comparisons of the radiative and autoionizing transition rates in Ref. [34] with the data produced by RELAC in the present work show good agreement for the strong radiative and autoionizing transitions, but large discrepancies for weaker autoionizing transitions. Care has been taken in the present work to account for CI as fully as possible in the autoionizing states of each argon ion. Thus EA through as many levels in the continuum of each ion as possible (Tables I and II) has been computed simultaneously,

with interaction allowed between all levels with common parity and total angular momentum. Calculations of the overall EA cross section for Ar^{7+} agree to between 30% and 15% with the recent work of Reed and Chen [15].

Mitnik and co-workers at the Hebrew University in Jerusalem in their work on EA in Cu- [21] and Zn-like [22] ions have pointed out that for energy levels with a large exchange contribution to the level energy ($3d^9 4s 4d^2 S_{1/2}$ and $3d^9 4s^2 4d^1 S_0$ in Cu- and Zn-like ions, respectively), if configuration interaction with higher- n levels along these series ($3d^9 4s n d^2 S_{1/2}$ and $3d^9 4s^2 n d^1 S_0$) is neglected, RELAC and CROSS greatly overestimate the total EA cross section through these energy levels. The Na- and Mg-like ions of interest to the present work present similar issues. We find that the EA rate coefficient through the $2p^5 3s 3p^2 S_{1/2}$ level in Na-like Ar^{7+} computed at a temperature equal to the ion's ionization energy is $8.29 \times 10^{-11} \text{ cm}^3 \text{ sec}^{-1}$ with full accounting of CI and $10.5 \times 10^{-11} \text{ cm}^3 \text{ sec}^{-1}$ without the effect of the higher- n members of the $2p^5 3s n p^2 S_{1/2}$ series. For the EA rate coefficient of the $2p^5 3s^2 3p^1 S_0$ level in Mg-like Ar^{6+} computed at a temperature equal to the ion's ionization energy, we find 7.15×10^{-11} and $8.80 \times 10^{-11} \text{ cm}^3 \text{ sec}^{-1}$ with and without the contribution of the higher- n members of the $2p^5 3s^2 n p^1 S_0$ series, respectively. The $2p^5 3s 3p^2 S_{1/2}$ and $2p^5 3s^2 3p^1 S_0$ energy levels in Na- and Mg-like ions, respectively, account for 25% and 32% of the total EA rate through the $2p^5 3s 3l'$ ($l' = s, p, d$) and $2p^5 3s^2 3l'$ ($l' = p, d$) configurations with the full CI treatment of the present work and 27% and 35% of the total EA rate through the $2p^5 3s 3l'$ and $2p^5 3s^2 3l'$ configurations when CI with higher n levels along the $2S_{1/2}$ and $1S_0$ series is neglected. For the EA rate coefficient through the individual levels, CI is found to have a strong effect; however, the sum of the EA rate coefficients through all autoionizing levels is affected by CI by $\leq 10\%$.

The levels considered for radiative stabilization of the collisionally excited (continuum) levels can strongly effect the autoionization branching ratios for all the argon ions in the present work. Reed, Chen, and Moores at Livermore [13–15] in their work on EA in Na-like ions and Mitnik *et al.* [21,22] in their work on EA in Cu- and Zn-like ions have pointed out that radiative stabilization of the autoionizing levels via decays to excited bound levels can be dominant over resonant stabilization to the ground level. This is seen to be the case in the present work; Table IV shows the branching ratios for autoionization from several Na- and Mg-like autoionizing levels considering only stabilization to the ground level of the initial ion, considering stabilization to the ground and singly excited nearby energy levels and considering the full spectrum of decays to the stable levels in our models. It is seen from the data in Table IV that decays to the low-lying, singly excited levels near the ground level have the largest effect on the calculated branching ratios. Note that the metastable $(2p_{3/2} 3s 3p_{3/2})_{7/2}$ Na-like level has an autoionization branching ratio of 1.000 in every case. For this level, autoionization probabilities are quite small (only a few high angular momentum partial waves of the outgoing electron are available), but the radiative stabilization rates (which do not proceed directly to the ground level or to the low-lying, singly excited levels near the ground level) are over five orders of magnitude smaller still.

TABLE IV. Autoionization branching ratio for inner-shell excited levels in Na- and Mg-like argon (Ground only) with only resonant stabilization, ($3l$, $l=s,p,d$) with stabilization to singly excited energy levels near the ground level, and (BR full) with stabilization to all bound states of the initial ion. The energy levels are indicated by a series of jj -coupling orbitals, where the first orbital is the inner-shell hole followed by occupied orbitals, and the total angular momentum of the level written as a subscript after the parenthesis followed by the calculated energy of the level.

Level name	Energy (eV)	Ground only	$3l$ ($l=s,p,d$)	BR full
Na-like (ionization potential 142.3 eV)				
$(2p_{3/2}3s^2)_{3/2}$	243.0	0.965	0.965	0.965
$(2p_{1/2}3s^2)_{1/2}$	245.2	0.965	0.965	0.965
$(2p_{3/2}3s3p_{1/2})_{3/2}$	254.5	1.000	0.780	0.778
$(2p_{3/2}3s3p_{3/2})_{7/2}$	256.5	1.000	1.000	1.000
$(2p_{3/2}3s3p_{1/2})_{5/2}$	256.7	1.000	0.881	0.881
$(2p_{3/2}3s3p_{1/2})_{3/2}$	257.1	1.000	0.624	0.621
$(2p_{3/2}3s3p_{1/2})_{1/2}$	257.6	1.000	0.009	0.009
$(2p_{3/2}3s3p_{3/2})_{5/2}$	258.1	1.000	0.850	0.848
$(2p_{3/2}3s3p_{3/2})_{3/2}$	258.5	1.000	0.520	0.517
$(2p_{1/2}3s3p_{1/2})_{1/2}$	258.8	1.000	0.327	0.330
$(2p_{1/2}3s3p_{3/2})_{3/2}$	259.6	1.000	0.669	0.667
$(2p_{3/2}3s3p_{3/2})_{1/2}$	259.9	1.000	0.310	0.306
$(2p_{1/2}3s3p_{3/2})_{5/2}$	260.4	1.000	0.593	0.591
$(2p_{1/2}3s3p_{1/2})_{3/2}$	260.5	1.000	0.276	0.274
$(2p_{1/2}3s3p_{1/2})_{1/2}$	261.0	1.000	0.977	0.977
$(2p_{3/2}3s3p_{3/2})_{5/2}$	265.0	1.000	0.953	0.953
$(2p_{3/2}3s3p_{3/2})_{3/2}$	265.9	1.000	0.865	0.864
$(2p_{1/2}3s3p_{3/2})_{3/2}$	267.6	1.000	0.899	0.898
$(2p_{1/2}3s3p_{3/2})_{1/2}$	267.7	1.000	0.987	0.987
$(2p_{3/2}3s3p_{3/2})_{1/2}$	272.1	1.000	1.000	1.000
Mg-like (ionization potential 121.5 eV)				
$(2p_{3/2}3s^23p_{1/2})_1$	247.9	1.000	0.998	0.998
$(2p_{3/2}3s^23p_{3/2})_3$	249.7	1.000	0.987	0.987
$(2p_{3/2}3s^23p_{1/2})_2$	249.8	1.000	0.981	0.981
$(2p_{3/2}3s^23p_{3/2})_1$	250.4	1.000	0.983	0.983
$(2p_{3/2}3s^23p_{3/2})_2$	250.9	1.000	0.832	0.832
$(2p_{1/2}3s^23p_{1/2})_1$	252.0	1.000	0.985	0.985
$(2p_{1/2}3s^23p_{1/2})_0$	252.0	1.000	0.985	0.985
$(2p_{1/2}3s^23p_{3/2})_2$	252.6	1.000	0.965	0.965
$(2p_{1/2}3s^23p_{3/2})_1$	252.6	1.000	0.978	0.978
$(2p_{3/2}3s^23p_{3/2})_0$	261.5	1.000	1.000	1.000
Na-like (ionization potential 142.3 eV)				
$(2p_{3/2}3s3d_{3/2})_{1/2}$	282.1	0.382	0.338	0.371
$(2p_{3/2}3s3d_{3/2})_{3/2}$	282.4	0.686	0.677	0.673
$(2p_{3/2}3s3d_{5/2})_{5/2}$	282.8	1.000	0.858	0.857
$(2p_{3/2}3s3d_{5/2})_{9/2}$	283.2	0.000	0.000	0.000
$(2p_{3/2}3s3d_{3/2})_{7/2}$	283.6	1.000	0.737	0.736
$(2p_{3/2}3s3d_{3/2})_{5/2}$	284.0	1.000	0.860	0.859
$(2p_{3/2}3s3d_{3/2})_{3/2}$	284.4	0.648	0.445	0.451
$(2p_{3/2}3s3d_{5/2})_{7/2}$	285.0	1.000	0.648	0.647
$(2p_{3/2}3s3d_{3/2})_{5/2}$	285.4	1.000	0.786	0.784
$(2p_{3/2}3s3d_{3/2})_{1/2}$	285.7	0.944	0.949	0.943

TABLE IV. (Continued).

Level name	Energy (eV)	Ground only	$3l$ ($l=s,p,d$)	BR full
$(2p_{3/2}3s3d_{5/2})_{3/2}$	285.9	0.813	0.778	0.790
$(2p_{1/2}3s3d_{5/2})_{5/2}$	286.5	1.000	0.887	0.887
$(2p_{1/2}3s3d_{3/2})_{3/2}$	287.0	0.994	0.985	0.987
$(2p_{1/2}3s3d_{5/2})_{7/2}$	287.1	1.000	0.888	0.887
$(2p_{1/2}3s3d_{5/2})_{5/2}$	287.5	1.000	0.539	0.537
$(2p_{1/2}3s3d_{5/2})_{3/2}$	287.6	0.999	0.998	0.998
$(2p_{1/2}3s3d_{3/2})_{3/2}$	289.9	0.992	0.992	0.992
$(2p_{1/2}3s3d_{3/2})_{1/2}$	290.1	0.993	0.993	0.993
$(2p_{3/2}3s3d_{5/2})_{7/2}$	291.3	1.000	0.995	0.995
$(2p_{3/2}3s3d_{5/2})_{5/2}$	292.2	1.000	0.987	0.987
$(2p_{3/2}3s3d_{5/2})_{3/2}$	293.3	0.998	0.997	0.997
$(2p_{1/2}3s3d_{3/2})_{5/2}$	294.0	1.000	0.983	0.982
$(2p_{1/2}3s3d_{5/2})_{1/2}$	294.0	0.996	0.996	0.996

Mg-like (ionization potential 121.5 eV)

$(2p_{3/2}3s^23d_{5/2})_4$	279.5	1.000	0.995	0.995
$(2p_{3/2}3s^23d_{3/2})_0$	279.9	1.000	1.000	1.000
$(2p_{3/2}3s^23d_{3/2})_3$	279.9	1.000	0.994	0.994
$(2p_{3/2}3s^23d_{3/2})_1$	280.0	1.000	1.000	1.000
$(2p_{3/2}3s^23d_{5/2})_2$	280.3	1.000	1.000	1.000
$(2p_{3/2}3s^23d_{3/2})_2$	280.5	0.999	0.995	0.995
$(2p_{3/2}3s^23d_{5/2})_3$	280.8	1.000	0.992	0.991
$(2p_{3/2}3s^23d_{5/2})_1$	281.7	0.989	0.986	0.986
$(2p_{1/2}3s^23d_{3/2})_2$	282.3	0.998	0.991	0.991
$(2p_{1/2}3s^23d_{5/2})_3$	282.5	1.000	0.993	0.992
$(2p_{1/2}3s^23d_{5/2})_2$	282.8	0.999	0.998	0.997
$(2p_{1/2}3s^23d_{3/2})_1$	283.4	0.996	0.996	0.996

E. Enhancement of direct ionization

The rates of impact ionization [26,27] from all of the energy levels listed in Table III have been computed. Both valence-shell and inner-shell ionization rates have been considered and the contributions have been summed to produce the total, direct, impact ionization rate. Energies for both the

valence- and inner-shell orbitals are computed by RELAC. The factor by which EA enhances the rate of direct ionization (DI) is given by

$$R(T_e) = \frac{S_i^{\text{EA}}(T_e) + S_i^{\text{DI}}(T_e)}{S_i^{\text{DI}}(T_e)}, \quad (20)$$

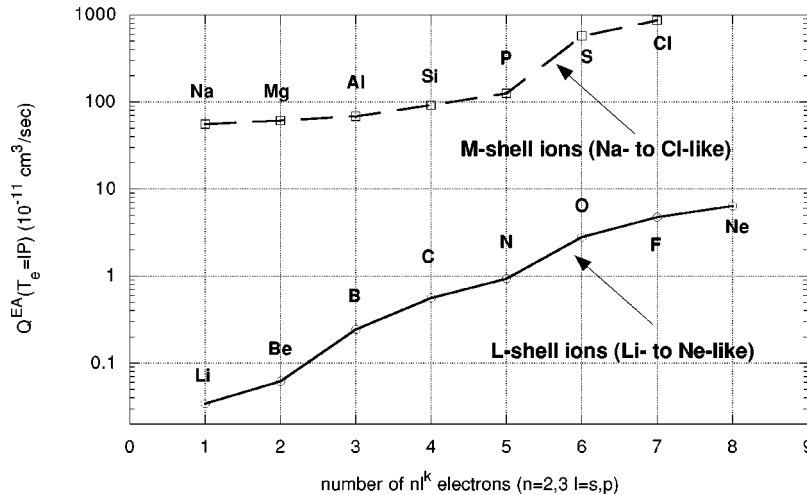


FIG. 10. EA rate coefficient for the ground level in each ion (computed at an electron temperature equal to each ion's ionization potential) versus the number of electrons in the outer shell ($n=2$ for the L shell, $n=3$ for the M shell).

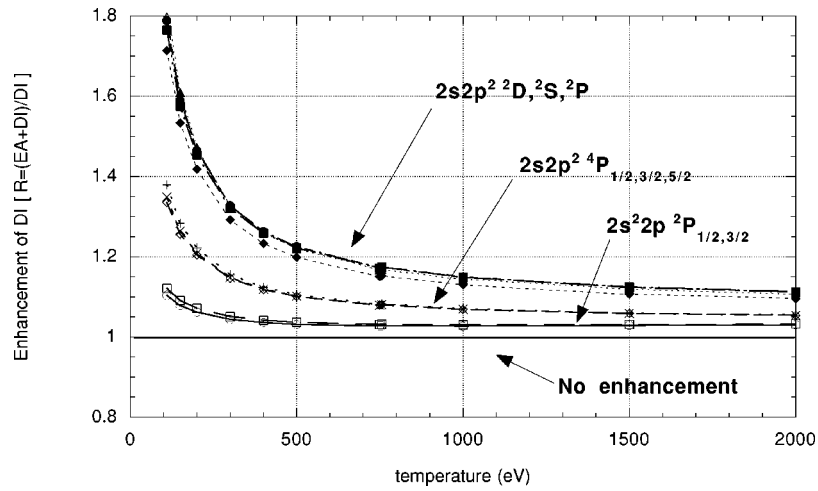


FIG. 11. Factor by which EA enhances direct ionization from the two $2s^2 2p$ levels and the eight $2s2p^2$ excited energy levels in B-like Ar^{13+} .

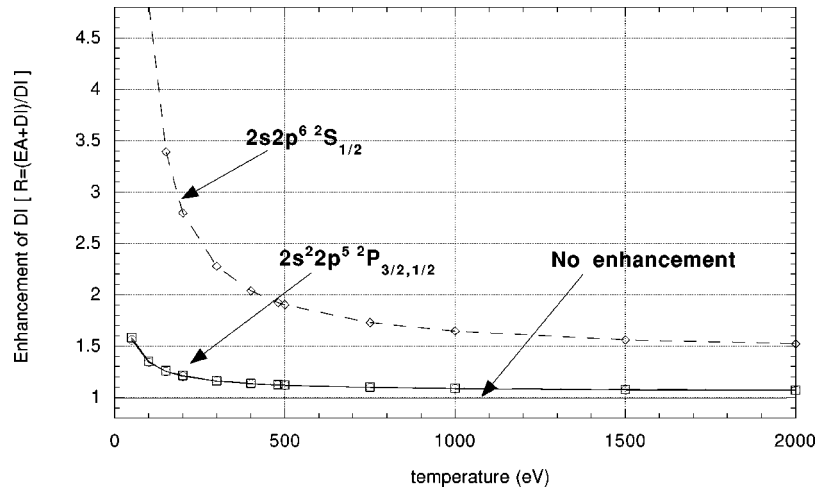


FIG. 12. Factor by which EA enhances direct ionization in the F-like Ar^{9+} $2s^2 2p^5$ levels and in the one level of the $2s2p^6$ first excited configuration.

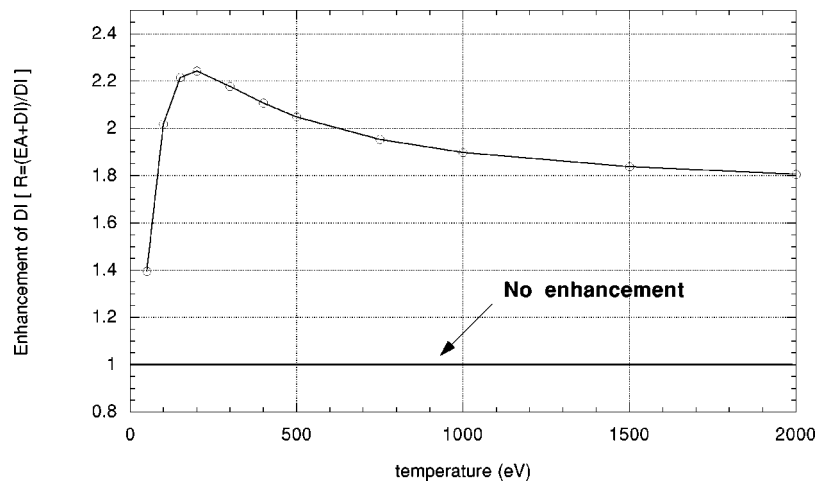


FIG. 13. Factor by which EA enhances direct ionization from the $3s$ ground level in Na-like Ar^{7+} .

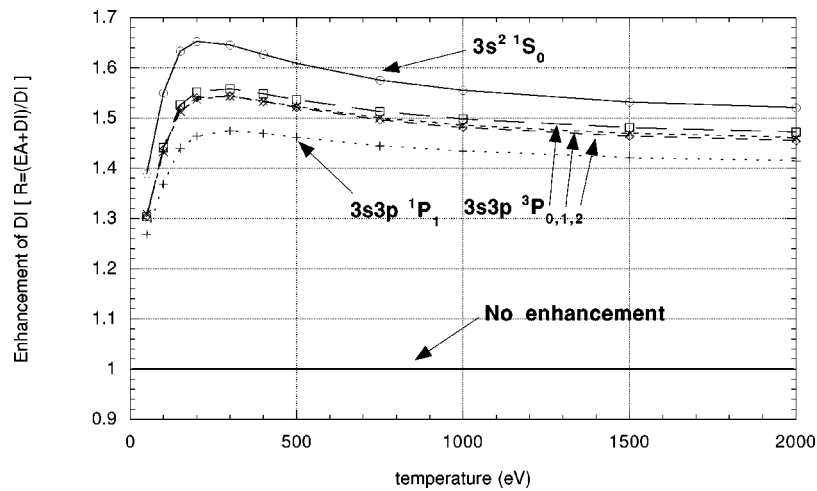


FIG. 14. Factor by which EA enhances direct ionization in the Mg-like Ar^{6+} $3s^2$ ground level and in the $3s3p$ ($^3P_{0,1,2}$ and 1P_1) excited levels.

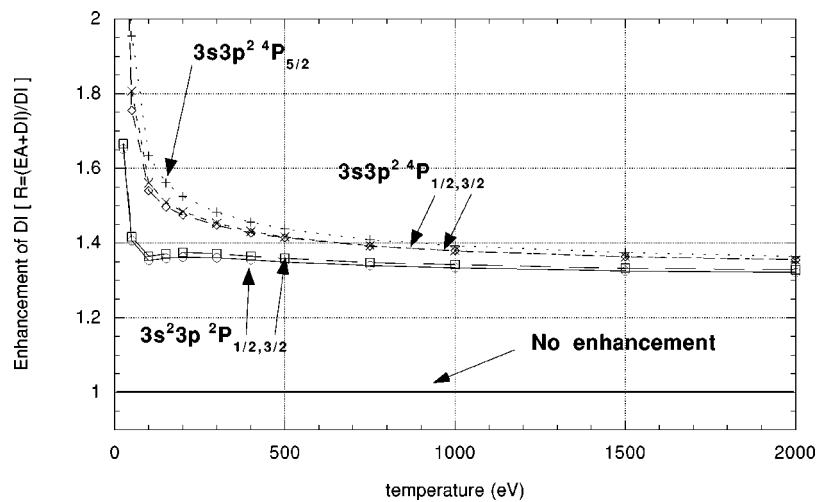


FIG. 15. Factor by which EA enhances direct ionization in the Al-like Ar^{5+} $3s^23p$ levels and in the three lowest-energy levels of the $3s3p^2$ first excited configuration.

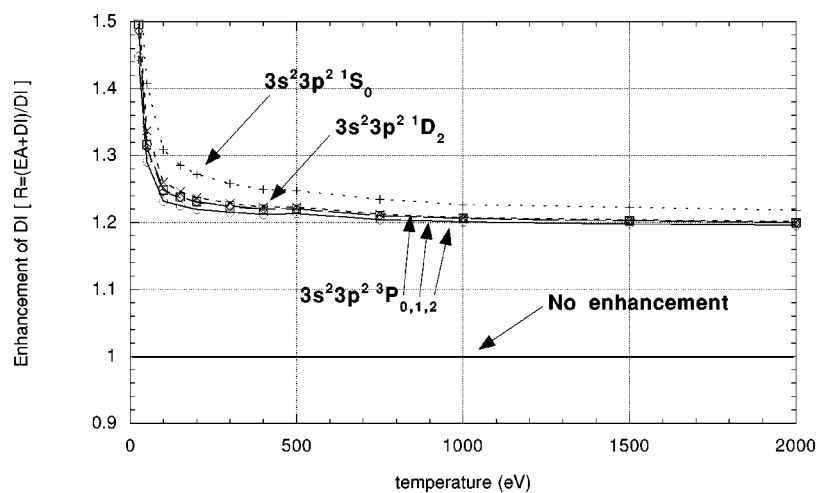


FIG. 16. Factor by which EA enhances direct ionization from the five $3s^23p^2$ levels in Si-like Ar^{4+} .

where $S_i^{\text{DI}}(T_e)$ is the rate coefficient for direct ionization. For B-like Ar¹³⁺ and F-like Ar⁹⁺, the factor by which EA enhances DI is shown in Figs. 11 and 12, respectively. For the ground levels of these two *L*-shell ions, it is seen that EA enhances the rate of DI by a small amount, $5\% \leq R(T_e) \leq 10\%$. In the Li- and Be-like ions, the enhancement is even smaller. The corresponding figure for the levels of the other *L*-shell argon ions look similar to Figs. 11 and 12. At low temperatures ($T_e \lesssim 1/2$ each ion's ionization potential), EA from the levels of the first excited configuration can significantly enhance DI and even exceed the rate of DI in the case of the F-like Ar⁹⁺ ion. The rate of EA also exceeds the rate of DI for the levels of the first excited configuration in O-like Ar¹⁰⁺.

The EA enhancement of direct ionization in Na-like Ar⁷⁺ is shown in Fig. 13. The enhancement of DI for the ground and excited levels in Mg-like Ar⁶⁺, Al-like Ar⁵⁺, and Si-like Ar⁴⁺ is shown in Figs. 14–16. It is seen that for Na-, Mg-, and Al-like ions, the rate of EA from the ground level introduces a large enhancement to the direct ionization rate, particularly at low temperatures. The low ionization energy of an *M*-shell electron in these ions compared to the ionization energy of an inner *2l* electron means that the number of *L*- and *M*-shell excitations that contribute to EA is large. In

the cases of the Al- and Si-like ions (Figs. 15 and 16), the ratio $R(T_e)$ turns up sharply at very low temperatures due to the dominance of the *M*-shell EA channel [Eqs. (13) and (14)]. The strong enhancement at very low temperatures of the direct ionization rate from the ground level is also seen in the P- and S-like argon ions. It is known that the Lotz formulas used to compute the DI rate coefficients in the present work overestimates the direct ionization cross section [2,24]; thus data displayed in Figs. 13–16 can be thought of as lower limits on the EA enhancement of the rate of DI. Since two of the four levels of the first excited configuration in Mg-like argon are metastable and the levels of the first excited configuration in Al-like argon are only ~ 10 eV above the ground level, the contribution of these level to the total ionization rate for these ions in the steady state (even for a relatively low-density plasma) must be taken into account in any plasma modeling exercise.

ACKNOWLEDGMENT

This work was performed under the auspices of the U.S. Department of Energy at the Lawrence Livermore National Laboratory under Contract No. W-7405-ENG-48.

-
- [1] D. H. Crandall, R. A. Phaneuf, B. E. Hasselquist, and D. C. Gregory, *J. Phys. B* **12**, L249 (1979).
- [2] D. H. Crandall, *Phys. Scr.* **23**, 153 (1981).
- [3] D. H. Crandall *et al.*, *Phys. Rev. A* **34**, 1757 (1986).
- [4] A. Müller *et al.*, *J. Phys. B* **13**, 1877 (1980).
- [5] S. Rachafi *et al.*, *J. Phys. B* **24**, 1037 (1991).
- [6] Y. Zhang *et al.*, *Phys. Rev. A* **45**, 2929 (1992).
- [7] R. D. Cowan and J. B. Mann, *Astrophys. J.* **232**, 940 (1979).
- [8] R. J. W. Henry, *J. Phys. B* **12**, L309 (1979).
- [9] D. H. Sampson and L. B. Golden, *J. Phys. B* **12**, L785 (1979).
- [10] D. H. Sampson and L. B. Golden, *J. Phys. B* **14**, 903 (1981).
- [11] K. LaGattuta and Y. Hahn, *Phys. Rev. A* **24**, 2273 (1981).
- [12] D. C. Griffin, M. Pindzola, and C. Botcher, *Phys. Rev. A* **36**, 3642 (1987).
- [13] K. J. Reed, M. H. Chen, and D. L. Moores, *Phys. Rev. A* **41**, 550 (1990).
- [14] K. J. Reed, M. H. Chen, and D. L. Moores, *Phys. Rev. A* **44**, 4336 (1991).
- [15] K. J. Reed and M. H. Chen, *Phys. Rev. A* **54**, 2967 (1996).
- [16] S. S. Tayal, *Phys. Rev. A* **49**, 2561 (1994).
- [17] H. Teng and Z. Xu, *Phys. Rev. A* **54**, 444 (1996).
- [18] H. Teng *et al.*, *J. Phys. B* **29**, 2209 (1996).
- [19] D. H. Sampson, *J. Phys. B* **15**, 2087 (1982).
- [20] D. Mitnik *et al.*, *Phys. Rev. A* **50**, 4911 (1994).
- [21] D. Mitnik *et al.*, *Phys. Rev. A* **53**, 3178 (1996).
- [22] D. Mitnik *et al.*, *Phys. Rev. A* **55**, 307 (1997).
- [23] K. B. Fournier *et al.*, *Phys. Rev. A* **54**, 3870 (1996).
- [24] M. Arnaud and R. Rothenflug, *Astron. Astrophys., Suppl. Ser.* **60**, 425 (1985).
- [25] M. Arnaud and J. Raymond, *Astrophys. J.* **398**, 394 (1992).
- [26] W. Lotz, *Z. Phys.* **216**, 241 (1968).
- [27] W. Lotz, *Z. Phys.* **232**, 101 (1970).
- [28] A. Bar-Shalom, M. Klapisch, and J. Oreg, *Phys. Rev. A* **38**, 1773 (1988).
- [29] A. Bar-Shalom and M. Klapisch, *Comput. Phys. Commun.* **50**, 375 (1988).
- [30] M. Klapisch, *Comput. Phys. Commun.* **2**, 239 (1971).
- [31] M. Klapisch, J. Schwob, B. Fraenkel, and J. Oreg, *J. Opt. Soc. Am.* **67**, 148 (1977).
- [32] I. P. Grant, *J. Phys. B* **7**, 1458 (1974).
- [33] J. Oreg, W. H. Goldstein, M. Klapisch, and A. Bar-Shalom, *Phys. Rev. A* **44**, 1750 (1991).
- [34] M. H. Chen, *Phys. Rev. A* **40**, 2365 (1989).